Adv Polym Sci (2011) 241: 1–55
DOI:10.1007/12_2010_104

Published online: 23 November 2010

Conformations and Solution Properties of Star-Branched Polyelectrolytes

Oleg V. Borisov, Ekaterina B. Zhulina, Frans A.M. Leermakers, Matthias Ballauff, and Axel H.E. Müller

Abstract Aqueous solutions of star-like polyelectrolytes (PEs) exhibit distinctive features that originate from the topological complexity of branched macromolecules. In a salt-free solution of branched PEs, mobile counterions preferentially localize in the intramolecular volume of branched macroions. Counterion localization manifests itself in a dramatic reduction of the osmotic coefficient in solutions of branched polyions as compared with those of linear PEs. The intramolecular osmotic pressure, created by entrapped counterions, imposes stretched conformations of branches and this leads to dramatic intramolecular conformational transitions upon variations in environmental conditions. In this chapter, we overview the theory of conformations and stimuli-induced conformational transitions in star-like PEs in aqueous solutions and compare these to the data from experiments and Monte Carlo and molecular dynamics simulations.

O.V. Borisov (✉)
Institut Pluridisciplinaire de Recherche sur, l'Environnement et les Matériaux,
UMR 5254 CNRS/UPPA, 064053 Pau, France
e-mail: oleg.borisov@univ-pau.fr
and
Institute of Macromolecular Compounds of the Russian Academy of Sciences, 199004
St. Petersburg, Russia

E.B. Zhulina
Institute of Macromolecular Compounds of the Russian Academy of Sciences, 199004
St. Petersburg, Russia

F.A.M. Leermakers
Laboratory of Physical Chemistry and Colloid Science, Wageningen University, 6703
Wageningen, The Netherlands

M. Ballauff
Humboldt Universität and Helmholtz-Zentrum Berlin für Materialien und Energie GmbH Berlin,
Germany

A.H.E. Müller
Makromolekulare Chimie II and Bayreuther Zentrum für Kolloide und Grenzflächen,
Universität Bayreuth, 95440 Bayreuth, Germany

Keywords Branched polyelectrolytes · Ionic fractals · Charge renormalization · Intra-molecular conformational transitions

Contents

1 Introduction

Ionic polymers constitute an important class of water-soluble macromolecules [1]. Synthetic polyelectrolytes (PEs) and polyampholytes have been in the focus of attention for many years. Most biomacromolecules (proteins, nucleic acids and polysaccharides) carry ionizable groups and are therefore included in this class of polymers. Ionic macromolecules have an ability to significantly change their conformations as a response to variations in the environmental conditions. This makes them interesting candidates for technological applications that range from nanomedicine and food production to paper making and oil recovery.

Highly intriguing and truly unique properties of PE solutions arise from an interplay between long-ranged electrostatic interactions and the chemical connectivity of ionic monomers in these polymer chains. Even though the basic understanding of properties of linear PEs has advanced during the past decade (see, for example, reviews [2, 3] and references therein), the corresponding insights for more complex macro- and supramolecular PE assemblies are less developed. Examples of such assemblies include colloidal PE brushes [4], ionic dendrimers [5], charged microgels [6], randomly [7] or regularly branched PEs [8, 9], and aggregates of amphiphilic ionic block copolymers [10].

Self-assembled nanostructures of biopolymers play an important role in nature. For example, extracellular branched polysaccharides decorate bacterial surfaces and therewith mediate cell adhesion [11], aggrecans (protein–polysaccharide complexes) control mechanical stresses in synovial joints [12], whereas neurofilaments (neuron-specific protein assemblies) support the elongated cell shape and participate in the maintenance of the axonal caliber [13]. It is believed that these biological functions rest on the ability of bioassemblies to provide adequate responses to variations in the local environment. Therefore, a better understanding of the physical mechanisms that govern conformational rearrangements in (bio)nanostructures, is of key importance, not only for colloid and material sciences, but also for cell biology.

The molecular organization of biopolymers is often much more complex than that of polymers synthesized in a chemical laboratory. Work is underway to systematically close this gap. Recent progress in controlled radical polymerization has made it possible to synthesize increasingly complex ionic macromolecules with controlled dimensions and topology. As a result, well-defined ionic block copolymers [10], colloidal [4] and molecular [8] PE brushes, and star-like PEs [9] have become available. In addition to emerging applications, such nanostructures constitute excellent model systems.

Star-shaped macromolecules exemplify generic features that result from the branched topology [14, 15]. Started by pioneering work of Stockmayer and Zimm [16], conformations of nonionic star-branched macromolecules were amply studied theoretically [16–20]. The fact that conformations of nonionic star-shaped polymers in dilute and semidilute solutions are determined by the repulsive short-range binary (in good solvent conditions) or ternary (in theta-solvent conditions) interactions between monomers has been demonstrated by more recent scaling models of Daoud and Cotton [21] and of Zhulina and Birhstein [22–24]. The equilibrium size of a star-like polymer (or simply star polymer) is determined by the conformations of its branches. These are controlled by the balance between intramolecular repulsive interactions, which induce stretching at the expense of conformational entropy losses.

Compared to short-ranged excluded-volume interactions, long-ranged intramolecular electrostatic repulsion has a much bigger impact on the conformations of the arms in ionic polymer stars. The Coulomb interactions in a PE solution are, however, always partially screened by small mobile counterions that are invariably present to ensure the electroneutrality of the system. The importance of nonlinear screening effects and of the counterion localization in solutions of strongly charged linear polyions, was first understood in terms of the Manning condensation [25].

In a dilute salt-free solution of branched PEs, the distribution of counterions is strongly inhomogeneous [26–35]. Similarly to strongly charged colloidal particles [36], branched PEs (stars, dendrimers, hyperbranched PEs, molecular and colloidal PE brushes) can maintain a high local electrostatic potential. The latter might be so strong that the attraction of mobile counterions to such macroion competes with their translational entropy. As a result, ions remain preferentially localized in the vicinity of macroions. In contrast to a classical solid colloidal particle, a branched PE macromolecule has a relatively low internal volume fraction of the monomer units and, therefore, these molecules can accommodate a huge fraction of its counterions in their volume. The escape of counterions into the bulk solution is discouraged by the strong Coulombic attraction to these highly branched (and thereby heavily charged) macromolecules. Because the internalized counterions retain some translational freedom, they generate an osmotic pressure. As a response to this pressure, a branched ionic macromolecule can stretch its arms, providing more space for the counterions. The equilibrium structure is thus the result of the balance between a restoring force in stretched arms and an osmotic one.

The concept of counterion localization in colloidal PE brushes and star-like PEs was first formulated on the basis of scaling arguments [26, 27], and later supported by a Poisson–Boltzmann-type analysis [27, 29, 37]. It has been further understood that the counterion localization and the osmotic swelling are generic properties of branched macroions, and that the onset of counterion localization occurs at a certain characteristic degree of branching for each particular polyion topology [31–33]. Unambiguous evidence of a clearly inhomogeneous distribution of counterions in solutions of star polyions, was provided by Monte Carlo [38] and molecular dynamics simulations [39–42]. A convincing experimental proof of the counterion localization, was given by osmotic pressure measurements in dilute salt-free solutions of PE star polymers [43] and colloidal PE brushes [44, 45].

Due to the counterion localization, conformations of branched macroions that comprise strongly dissociating groups (charge is quenched) are almost insensitive to the addition of salt, up to relatively high salt concentrations. The ability of a branched polyion to maintain a virtually constant ionic strength in its interior is of special interest for potential applications, where a controlled (buffered) microenvironment is essential (e.g., colloidal bionanoreactors, smart nanocontainers for biologically active molecules, etc.).

In quenched PE stars, the degree of dissociation is hardly affected by the proton concentration inside the macroion volume. In contrast to this, in a weakly dissociating (charge is annealing) branched macroion, the degree of ionization is affected by the local intramolecular proton concentration, which may differ from that in the bulk. The change in charge density in the PE star has a corresponding effect on the charge compensation by the counterions. Annealing PE stars, therefore, have peculiar responsive properties, e.g., they exhibit a non-monotonic variation of their size as a function of the ionic strength in the solution [28, 30].

Experimental studies of solutions of PE star polymers are rare, because the synthesis of macromolecules with a controlled number and length of branches still presents a significant challenge. A few recent studies report on various properties

of solutions of star-branched PEs, in which the number of arms was systematically varied [43, 46–51]. A number of studies on the pH and salt response, has been performed on star-like micelles with a PE corona and a kinetically frozen hydrophobic core [52–63]. These micelles mimic many-armed PE stars, although the number of arms (equal to the micelle aggregation number) is poorly controlled.

The objective of this chapter is to present an overview of the existing theories on conformations of star-branched PEs and to compare these to experimental data and the results of computer simulations. Some emphasis is made on the effect of counterion localization and its consequences for the conformations of branched PEs.

We start with a brief reminder on the scaling theory of nonionic star-branched polymers (Sect. 2), and proceed with the scaling model of a PE star polymer in a salt-free dilute solution (Sect. 3). We then discuss the physical basis of counterion localization and its manifestation in branched PEs of different topologies (Sect. 4).)

A quantitative analysis of counterion localization in a salt-free solution of star-like PEs is carried out on the basis of an exact numerical solution of the corresponding Poisson–Boltzmann (PB) problem (Sect. 5). Here, the conformational degrees of freedom of the flexible branches are accounted for within the Scheutjens–Fleer self-consistent field (SF-SCF) framework. The latter is used to prove and to quantify the applicability of the concept of colloidal charge renormalization to PE stars, that exemplify "soft" charged colloidal objects. The predictions of analytical and numerical SCF–PB theories are complemented by results of Monte Carlo (MC) and molecular dynamics (MD) simulations. The available experimental data on solution properties of PE star polymers are discussed in the light of theoretical predictions (Sect. 6).

Finally, an analytical theory of conformations of highly branched PE stars is discussed (Sect. 7). The predictions are critically compared to numerical SCF–PB results. Here we focus on the responsive properties of strongly and weakly dissociating PE star polymers, e.g., their ability to change their conformations in response to a varied ionic strength and pH in solution. Inferior solvent quality triggers conformational transitions in PE star polymers (Sect. 8). Relevant theoretical insights are reviewed and compared to MD simulation results.

2 Solutions of Neutral Star Polymers: Reminder on the Scaling Theory

We start with a brief review of the theory for conformational and solution properties of neutral (uncharged) star-branched polymers.

Consider a star polymer, composed of p linear arms, each arm with a length of N monomers. As shown in Fig. 1, a star comprises a central "core" domain onto which the linear arms are grafted by one of their ends. The effect of a finite core size on the star characteristics is negligible, as long as the dimensions of extended arms exceed, by far, that of the core. The arms of the star are assumed to be intrinsically flexible, so that the Kuhn length is on the order of monomer size a.

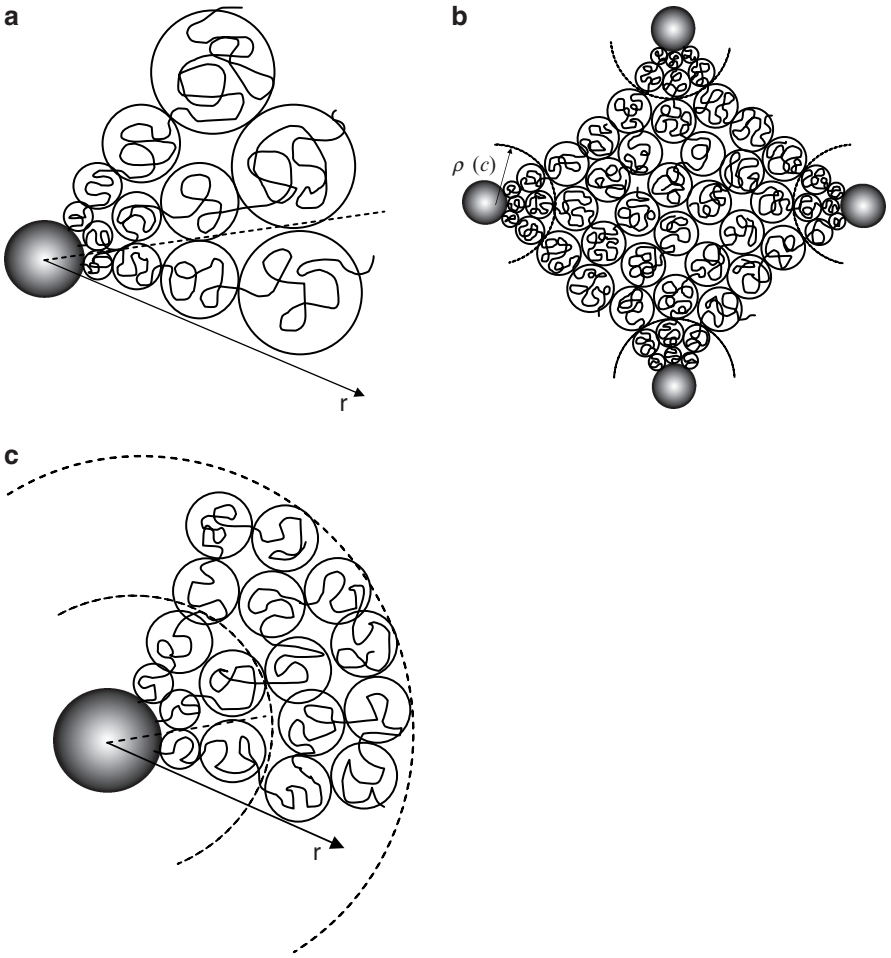

Fig. 1 Blob model for nonionic polymer stars: a single star under good or theta-solvent conditions (**a**), semidilute star solution (**b**), single polymer star partially collapsed in poor solvent (**c**). r distance from the center of the star

In the classical theory of Stockmayer and Zimm [16], a star polymer consists of p ideal (Gaussian) non-interacting branches, linked together in the center of the molecule. This model can be used to evaluate the decrease in the size of a star polymer (e.g., in its radius of gyration), as compared with that of a linear macromolecule with the same degree of polymerization pN. The theory further developed by Benoit presents an estimate for the form factor, explaining the scattering of radiation by a dilute solution of (ideal) star polymers [17, 18]. Because interarm interactions are neglected in this model (i.e., the arms are treated as independently fluctuating ideal coils), the overall size of the star is systematically underestimated.

Short-range interactions (van der Waals attraction and hard-core repulsion) between monomers can be accounted for using a virial expansion. As long as the volume fraction of monomers in a star polymer is significantly below unity, only pairwise monomer–monomer interactions, with second virial coefficient $\upsilon \sim a^3(1-2\chi(T))$, or ternary interactions, with third virial coefficient $w \sim a^6$, are relevant. The former depends on the Flory–Huggins parameter χ and is positive under good solvent ($\chi < 1/2$) and negative under poor solvent conditions ($\chi > 1/2$). In a good solvent, binary interactions are dominated by the repulsive part of the monomer–monomer interaction potential (hard-core repulsion), whereas in a poor solvent, binary interactions are attractive (due to the van der Waals forces). A special case $\upsilon = 0$ (vanishing net binary interactions) corresponds to theta-solvent conditions, where weak attraction between monomers is exactly compensated by their excluded volume.

Subsequent theoretical studies [19, 20] have incorporated short-range monomer–monomer interactions using the mean field approximation, but systematically underestimated conformational entropy losses in the stretched arms. These theories thus overestimate the star size.

The first theories that implemented a proper balance of intramolecular interactions and conformational elasticity of the branches were developed by Daoud and Cotton [21] and by Zhulina and Birshtein [22–24]. These theories use scaling concepts (the blob model), originally developed by de Gennes and Alexander to describe the structure of semidilute polymer solutions [64] and planar polymer brushes [65, 66]. Here, the monomer–monomer interactions were incorporated on the level of binary or ternary contacts (corresponding to good and theta-solvent conditions, respectively), and both dilute and semidilute solutions of star polymers were considered. Depending on the solvent quality and the intrinsic stiffness of the arms, the branches of a star could be locally swollen, or exhibit Gaussian statistics [22–24].

2.1 Star Polymer Conformation in a Dilute Solution

According to the blob model, a flexible neutral star polymer can be envisioned as an array of concentric shells of closely packed blobs. For a visualization of the blobs, see Fig. 1a. The chain ends are assumed to be localized at the edge (i.e., within the outermost blobs), and each chain contributes one blob to each shell. The chain segment inside a blob remains unperturbed by the interactions with other branches and, therefore, exhibits Gaussian or excluded-volume statistics under theta- or good solvent conditions, respectively. For transparency, we consider first athermal, $\upsilon \cong a^3$, and theta-solvent, $\upsilon = 0$, conditions. The blob size at distance r from the star center is equal to the average interchain separation $\cong r/p^{1/2}$, which coincides with the local correlation length, $\xi(r)$. The latter is related to the local polymer concentration, $c_p(r)$, by the same scaling law as in a semidilute polymer solution, $\xi(r) \cong a[c_p(r)a^3]^{-\nu/(3\nu-1)}$, where ν is the Flory exponent ($\nu \approx 3/5$ and

$\nu = 1/2$ under good and theta-solvent conditions, respectively). Hence, the blob picture enables one to derive the power law for the radial decay in polymer density:

$$c_{\mathrm{p}}(r) \cong (p^{1/2}a/r)^{(3\nu-1)/\nu}a^{-3} \tag{1}$$

Here and below, the sign "$\cong$" implies that a numerical coefficient on the order of unity, is omitted.

The radial decay in polymer density corresponds to a radial decrease in local stretching of the arms, $\mathrm{d}r/\mathrm{d}n \cong p/[r^2 c_{\mathrm{p}}(r)] \cong a(p^{-1/2}r/a)^{(\nu-1)/\nu}$. At the same time, the local stretching of the branches controls the elastic tension and, thereby, the size of the elastic blob [67], $\xi_{\mathrm{elastic}} \cong a(a\mathrm{d}n/\mathrm{d}r)^{\nu/(1-\nu)}$. Within the blob picture, $\xi_{\mathrm{elastic}}(r) \cong \xi(r)$. Hence, the radial increase in the size of the concentrational blob, $\xi(r)$, also ensures the decrease in local tension in the arms of the star, $\xi_{\mathrm{elastic}}^{-1} \cong p^{1/2}/r$.

Making use of the normalization condition for the density profile:

$$4\pi \int_0^R c_{\mathrm{p}}(r) r^2 \mathrm{d}r = pN \tag{2}$$

one obtains a scaling expression for the overall size R of a star polymer:

$$R \cong aN^{\nu}p^{(1-\nu)/2} \tag{3}$$

As follows from (3), the star size, R, depends on the degree of polymerization, N, of the individual arms, with the same power law as that for a linear polymer chain, $R \sim N^{\nu}$. However, the repulsion between the branches of the star leads to the extension of its branches in the radial direction, as compared with the dimensions of an individual linear chain with the same degree of polymerization N. This cooperative effect of interbranch repulsion is described by the factor $p^{(1-\nu)/2}$ in (3). Because of the relatively high monomer concentration in the intramolecular volume of the star, the extension of its arms occurs even under theta-solvent conditions. In contrast to a linear polymer, the repulsion due to ternary monomer–monomer contacts inside the star ensures the stretching of its branches with respect to the Gaussian dimension. Remarkably, if the solvent is marginal good, the corona of a star with sufficiently long arms consists of two regions. In the central (theta) region, the chain segments within the blobs retain Gaussian statistics, and the density profile decays here as $c_{\mathrm{p}}(r) \cong p^{1/2}(wa^{-6})^{-1/4}a^{-2}r^{-1}$. Closer to the star periphery, the blobs become sufficiently large and swollen the density profile acquires a shape that is typical for a good solvent, $c_{\mathrm{p}}(r) \cong p^{2/3}\upsilon^{-1/3}a^{-2/3}r^{-4/3}$. The boundary between these regions, r_θ, is determined by the condition $\xi(r_\theta)\upsilon a^{-4} \cong 1$, i.e., $r_\theta \cong p^{1/2}\upsilon^{-1}a^4$. On the scale of the star as a whole, the crossover from the theta-regime to the good solvent regime can be estimated from the condition of swelling of the outermost coronal blob, $\xi(R)\upsilon a^{-4} \geq 1$, and implies $N\upsilon^2 p^{-1/2}a^{-6} \geq 1$. The overall star size R is then given by:

$$R \cong \begin{cases} aN^{3/5}(\upsilon/a^3)^{1/5}p^{1/5}, & \text{good solvent} \\ aN^{1/2}(w/a^6)^{1/8}p^{1/4}, & \text{theta-solvent} \end{cases} \tag{4}$$

The scaling arguments presented above capture the essential features of a neutral star polymer both in good and theta-solvent conditions: there is a power law decay of the radial monomer density and there are scaling dependencies for the overall star size R on number of branches p and the degree of polymerization N. These scaling predictions were tested by MD and MC simulations [68–72] and experimentally [73–79]. Although certain discrepancies were detected (see, e.g., the discussion in [72]), a simple blob model remains an important theoretical tool for interpreting experimental data on nonionic star macromolecules. A similar blob Ansatz, however, cannot be directly applied to the case when long-ranged electrostatic interactions come into play.

2.2 *Effects of Concentration and Interactions Between Polymer Stars*

Interactions between star polymers in dilute solutions were considered by Witten and Pincus [80, 81] using a scaling approach. According to the scaling model, the intermolecular repulsion between two star polymers arises at distance $d \leq 2R$ between their centers, due to the overlap of the coronae. The interactions are described by a "soft" binary repulsive potential $U_{\text{star}}(d)/k_{\text{B}}T \cong p^{1/2} \ln(2R/d)$ in both good and theta-solvents. The corresponding second virial coefficient of interaction between two nonionic stars scales as $\cong R^3$. A more complex analytical expression for the interaction potential interpolating between the logarithmic behavior at $d \leq 2R$ and the Yukawa form at $d \geq 2R$ has been suggested in [82] to fit the experimental data on scattering from star polymer solutions. The structure factor of a dilute solution of star polymers can be approximated by that of a solution of soft spheres [82, 83].

There are relatively few experimental studies on the interactions between star polymers. Therefore, to date, MD simulations have mostly been used to validate theoretical models. A comprehensive comparison between theoretical and experimental results has recently been reviewed by Jusufi and Likos [84].

Beyond the overlap concentration threshold, $c \geq c^* \cong pN/R^3$, star polymers form a semidilute solution. Because of the fact that the arms in a star are stretched, the scaling theory [24] predicts that the properties of semidilute solutions of star polymers are distinctively different from those of linear polymers. When the polymer concentration $c \geq c^*$, a semidilute solution is envisioned as a system of closely packed and virtually non-interpenetrating (segregated) polymer stars. A further increase in polymer concentration leads to a progressive contraction of the coronae of the individual stars. This contraction results in an increase in the conformational entropy of the partially stretched star arms.

The blob picture of a semidilute solution of polymer stars is schematically presented in Fig. 1b. The peripheral (contracted) regions of the star coronae are envisioned as a "sea of blobs" of constant size, which corresponds to a constant polymer concentration in this region. In contrast to this, within radius $\rho(c) \leq R$, the structure of the corona of individual stars is preserved (a system of growing

in radial direction blobs). Remarkably, the segments of star branches in the sea of blobs remain stretched up to relatively high polymer concentrations [24]. The local stretching of the arms decreases monotonously with increasing distance r from the center of the star. The interpenetration of the stars occurs at the periphery of the coronae, where the terminal segments of the arms in the sea of blobs lose stretching with respect to the Gaussian dimensions. An increase in the concentration, c, leads to the decrease in both $\rho(c)$ and overall star size R and, progressively, there is an increase of the interpenetration.

The conformational structure of stars in a semidilute solution regime is mirrored by the corresponding thermodynamic consequences. There is, e.g., a discontinuity in the osmotic compressibility near c^* [81]. The intensity of scattered radiation (normalized by the polymer concentration) exhibits a pronounced correlation peak, as a function of the scattering vector, in both dilute and semidilute regimes close to the overlap concentration c^*. The evolution of the correlation peak in these scattering curves has a remarkable dependence on the polymer concentration: its magnitude increases below, and decreases above c^*. The latter is due to the increasing interpenetration of the coronae and the decreasing size of the unperturbed central region of the stars [86, 87]. The theory of scattering from semidilute solutions of star polymers was developed in [85–87].

Only at a sufficiently high polymer concentration, when the dimensions of the arms approach those of individual linear chains in a semidilute solution at the same concentration, do the star coronae become fully interpenetrated and the correlation peak in the scattering curves disappears. In this concentration regime, the thermodynamic properties of the solution of branched macromolecules become similar to those of linear chains.

3 Cell Model of the Salt-Free Solution of Polyelectrolyte Stars

We will now focus on star polymers that carry charges, and introduce a cell model for a dilute solution of such macromolecules. To this end, we consider a PE star that occupies the central region of a spherical cell of radius $D \geq R$, as shown in Fig. 2. The cell comprises at least the corresponding number of mobile monovalent counterions that compensate the charge of the PE star, and additional salt may be included. Typically, the ion concentrations are different in the intrastar volume, $0 \leq r \leq R$, and in the exterior part of the cell, $R \leq r \leq D$. We will first focus on the case that no salt is added to the cell, and thus only counterions participate in the partial screening of long-ranged electrostatic interactions. A fraction α of the monomers in a PE star is electrically charged (ionized). If the Bjerrum length $l_B = e^2/\epsilon k_B T$ is on the order of monomer size a, the condition of weak charging, $\alpha \leq 1$, implies that a local stiffening of the arms due to the intraarm Coulomb repulsion can be neglected [2, 88, 89]. The "bare" charge of the star-branched polyion is $Qe = p\alpha Ne$, where e is the elementary charge.

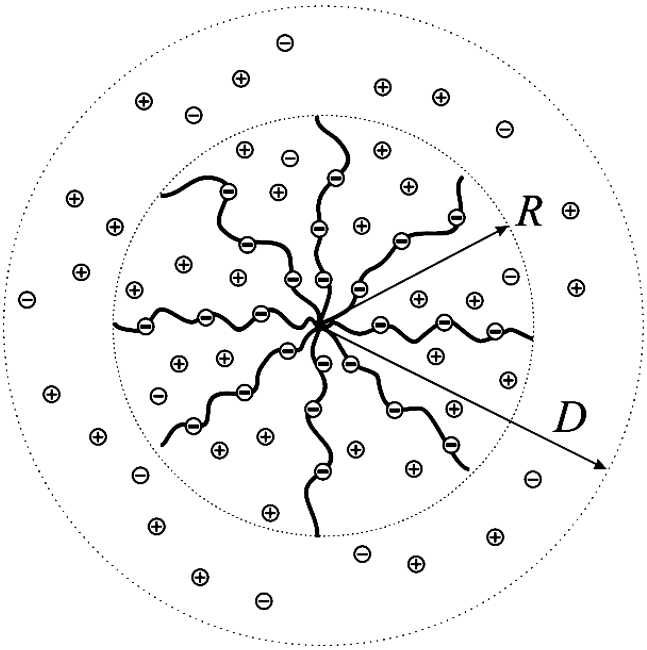

Fig. 2 Anionic star PE with eight arms having a radius R in 1:1 electrolyte solution (as indicated by the small spheres that carry a *plus* or a *minus* sign) in a spherical electroneutral Wigner–Seitz cell with radius D

We will distinguish between strongly and weakly ionizable PEs. In the former case, the fraction $\alpha \leq 1$ of "permanently" ionized monomers is quenched and determined by the chemical sequence in the arms. Environmental conditions, such as the pH and the local ionic strength, have a negligible effect on the charge of these quenched PEs. Partially sulfonated poly(styrene) (PSS) or partially quaternized poly(4-vinylpyridine) (PVP) are typical examples of a quenched polyanion and a polycation, respectively.

In the case of weakly ionizable PEs, the fraction of charged monomer units, α, is controlled by an ionization equilibrium and is affected by the local proton concentration and ionic strength. Weak polyacids such as poly(acrylic acid) (PAA) and poly(methacrylic acid) (PMAA), or polybases such as PVP and poly(dimethylaminoethyl methacrylate)(PDMAEMA) are typical examples of these pH-sensitive or "annealing" PEs.

Each monomer of a weak polyacid can be ionized via the dissociation of a hydrogen ion, H^+. The degree of dissociation of such acidic monomer, $\alpha(\mathbf{r})$, depends on the local concentration of hydrogen ions, $c_{\mathrm{H}^+}(\mathbf{r})$, via the mass action law:

$$\frac{\alpha(\mathbf{r})}{1-\alpha(\mathbf{r})} = \frac{K_{\mathrm{a}}}{c_{\mathrm{H}^+}(\mathbf{r})} \tag{5}$$

where K_a is the acidic ionization constant for an isolated monomer. For a polybase, the ionization occurs through the protonation of the monomers, and the generalization of the theory for this case is straightforward.

Remarkably, for branched PEs, which are characterized by a high intramolecular concentration of ionized monomers and, consequently, by a high intramolecular electrostatic potential, the value of the pH (here defined as minus the logarithm of the local proton concentration) in the intramolecular volume may differ significantly from that in the surrounding solution. Moreover, because of the connectivity of the charged monomers in the branches of the star, the local (excess) electrostatic potential created by neighboring monomers along a given arm is even larger than the average intramolecular one. The chemical connectivity of charges can be accounted for via an effective dissociation constant of a monomer, $K_a^{\text{eff}} \leq K_a$. However, in our subsequent discussion, we disregard these effects in the branches and only allow for radial gradients in the (average) intramolecular electrostatic potential, i.e., we will assume that $c_{H^+}(\mathbf{r}) = c_{H^+}(r)$ and $\alpha(\mathbf{r}) = \alpha(r)$.

3.1 Box-Like Cell Model of a Polyelectrolyte Star

The box-like cell model of a PE star can be considered as a generalization of a classical mean-field Flory approach, which was first suggested to describe the swelling of a polymer chain in a good solvent [90]. The Flory approach estimates the equilibrium dimensions of a macromolecule, as a function of its parameters, by balancing the free energy of intramolecular (repulsive) interactions with the conformational entropy loss of a swollen chain. Within the box-like approximation, the star is characterized by the radius of its corona, R (end-to-end distance of the arms), or by the average intramolecular concentration of its monomers:

$$c = \frac{3}{4\pi}\frac{pN}{R^3} \tag{6}$$

where radial gradients in polymer density, degree of ionization of the arms, and distributions of small ions are disregarded.

The free energy of the star is:

$$F = F_{\text{conf}} + F_{\text{ev}} + F_{\text{Coulomb}} + F_{\text{ions}} \tag{7}$$

Provided that the arms remain stretched with respect to their Gaussian size, $R \geq aN^{1/2}$, the conformational free energy of p uniformly stretched Gaussian chains (arms) is:

$$F_{\text{conf}}/k_BT = p\frac{3R^2}{2Na^2} = p\frac{3}{2Na^2}\left(\frac{3Np}{4\pi c}\right)^{2/3} \tag{8}$$

The free energy of non-electrostatic interactions is, within the virial expansion, given by:

$$F_{\text{ev}}/k_BT = pN\left(\upsilon c + wc^2\right) \tag{9}$$

In the absence of charges, or at a low degree of ionization of the arms, the star conformation is controlled by a balance between two first terms in (7) (i.e., the short-range interarm repulsions and the conformational entropy of stretched arms). As a result, the star size is given by (4). That is, the power law dependencies, obtained on the basis of the blob model, are recovered. The physical reasons why there is a match of the star size as obtained by the scaling and in the mean field approximations are discussed in details in [23].

3.2 Polyelectrolyte Star Conformation in a Dilute Salt-Free Solution

The box-like model allows for a straightforward analysis of the counterion localization, which is essential for understanding the specific properties of salt-free solutions of branched PEs. In the case of a PE star, the first two terms in the free energy in (7) are complemented by a contribution due to Coulomb interactions between all the charges (charged monomers and mobile ions) in the cell, F_{Coulomb}, and by the translational entropy of all mobile ions, F_{ions}. Following the line of arguments of [27, 29], we first focus on the case when no salt is added, and the cell contains only mobile (monovalent) counterions, which compensate the net charge of the star polyion. We assume that $Q^* \leq Q$ counterions are localized in the outer volume of the cell, $R \leq r \leq D$, whereas the remaining $(Q - Q^*)$ counterions are retained inside the star volume ($0 \leq r \leq R$). In the framework of the box-like model, the counterion concentration is assumed to have constant (but different) values inside and outside the star: $c_{\text{ions}}^{(\text{in})} = 3(Q - Q^*)/4\pi R^3$ and $c_{\text{ions}}^{(\text{out})} = 3Q^*/4\pi(D^3 - R^3)$, respectively. The entropic term in the free energy is, therefore, given by:

$$F_{\text{ions}}/k_{\text{B}}T = (Q - Q^*)\ln c_{\text{ions}}^{(\text{in})} + Q^* \ln c_{\text{ions}}^{(\text{out})} \tag{10}$$

and the Coulomb interaction term is given by:

$$F_{\text{Coulomb}}/k_{\text{B}}T = l_{\text{B}}\frac{Q^*}{R}\vartheta(R/D) \tag{11}$$

where $l_{\text{B}} = e^2/\epsilon k_{\text{B}}T$ is the Bjerrum length and $\vartheta(x)$ is a rational function of x, whose form is specified in [27, 29]. At the limit, when the cell size far exceeds the star size, $x = R/D \to 0$, $\vartheta(x) \to 3/5$. The minimization of the free energy, (7), (8), (9), (10), and (11), results in equilibrium values of the star size, R, and that of the uncompensated charge, Q^*. The latter is of special interest and can be found from the equation:

$$Q^* = \frac{R}{l_{\text{B}}}\frac{1}{2\vartheta(R/D)}\ln\left[\left(\frac{Q}{Q^*} - 1\right)\left(\frac{D^3}{R^3} - 1\right)\right] \tag{12}$$

It follows from the analysis of (12) that, in the limit of dilute solutions $D \gg R$, the distribution of counterions is governed by the parameter $l_B Q/R$, which is proportional to the dimensionless excess electrostatic potential (in units $k_B T/e$) created by the bare charge, $Q^* \approx Q$ of the star. When $Ql_B/R \ll 1$, the Coulomb attraction of counterions to the star polyion is weak compared to the thermal energy $k_B T$, and the counterions are distributed fairly uniformly in the solution. The uniform distribution optimizes the translational entropy for the ions. As a result, in the limit of dilute solutions, $D \gg R$, the fraction of counterions found in the intramolecular volume of the star is negligible, $Q^* \approx Q$, and the charged monomers in the branches interact via unscreened Coulomb repulsion. Balancing the Coulomb energy, (11), with the conformational penalty for the extension of the branches, (8), and neglecting the contributions due to non-electrostatic monomer–monomer interactions, (9), one obtains:

$$R \cong aN(\alpha^2 l_B/a)^{1/3} p^{1/3} \tag{13}$$

According to (13), the arms of the star are stretched proportionally to their degree of polymerization N, similarly to linear PEs in a dilute salt-free solution [91, 92]. The additional factor, $p^{1/3} \geq 1$, reflects the interarm Coulomb repulsion. A comparison to (4) shows that long-ranged interbranch Coulomb repulsion has a much stronger effect on the size of a PE star than the short-range interbranch repulsion that is found in a neutral star.

As follows from (13), the ratio Ql_B/R increases upon an increase in the number of arms p, because the star size $R \sim p^{1/3}$ grows less fast than the bare charge $Q \sim p$. The excess electrostatic potential becomes on the order of $k_B T/e$ at $p \cong \alpha^{-1/2}(l_B/a)^{-1}$. Increasing the number of arms above this value causes the excess electrostatic potential to become sufficiently strong that it will retain the majority of counterions within the intramolecular volume. Indeed, as follows from (12), when $Ql_B/R \gg 1$, the number of counterions released from the intrastar volume (and, correspondingly, the uncompensated charge Q^* of the star), scales as $Q^* \cong R/l_B$, and increases only logarithmically with Q. When $Q \gg Q^* \cong R/l_B$, one can neglect F_{Coulomb} and the second term in (10), and find the size of the star by balancing the translational entropy of $Q - Q^* \approx Q$ counterions, which are confined inside the intrastar volume, with the conformational entropy of the stretched arms. This leads to the expression:

$$R \cong aN\alpha^{1/2} \tag{14}$$

which can also be interpreted as a result of balancing the osmotic pressure of the confined counterions with the elastic (entropic) force that arises from stretching the arms. A striking feature of (14) is the absence of a power law dependence of the star size R on the number of arms p. In the limit of dilute solutions, $D \gg R$, an equation for the star size, which interpolates between the $Ql_B/R \ll 1$ and $Ql_B/R \gg 1$ limits (i.e., takes into account the contributions of both the Coulomb repulsions and the osmotic pressure of counterions), is given by:

$$R \cong a(N/p)^{1/3}[Q^{*2} l_B/5a + R(Q - Q^*)a^{-1}]^{1/3} \tag{15}$$

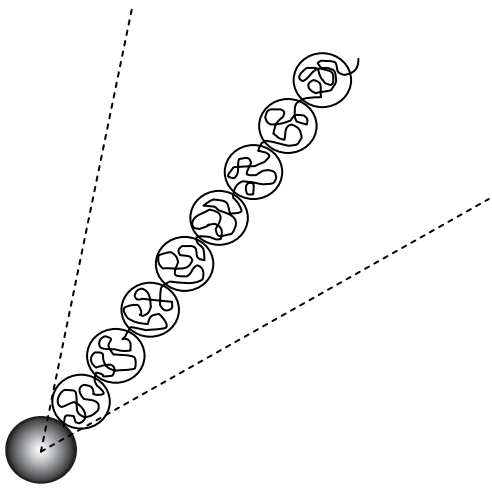

Fig. 3 Blob model of a PE star in salt-free solution

Remarkably, in a salt-free solution of the PE stars, the star size is found to be proportional to N, i.e., $R \sim N$, for both considered regimes. As a result, each arm can be envisioned as a string of elastic blobs of constant (independent of r) size [27], $\xi_{\text{elastic}} \cong a(\alpha^2 l_{\text{B}}/a)^{-1/3}$ and $\xi_{\text{elastic}} \cong a\alpha^{-1/2}$, in the regimes of unconfined and confined counterions, respectively. Hence, in contrast to the blob picture of a neutral star, the blobs in a PE star are not close-packed in a salt-free solution (see Fig. 3 for a schematic drawing).

3.3 Charge Renormalization Concept

The idea of counterion confinement (charge renormalization), is of central importance in understanding the properties of salt-free solutions of branched PEs. The concept was first formulated for a dilute salt-free solution of spherical charged colloidal particles by Alexander et al. [36]. It is illustrative to repeat the arguments briefly. Let us consider a dilute salt-free solution of charged colloidal particles with radius R_{c} and (positive) charge eQ. Counterions are distributed non-uniformly in the solution, with the highest concentration near the surface of the particles. If one applies a cell model, in which each particle is placed at the center of a regular Wigner–Seitz cell (approximated as a sphere), the osmotic pressure in the solution is determined by the counterion concentration at the cell boundary. The distribution of the electrostatic potential and that of the counterions within the cell (in the range $R_{\text{c}} \leq r \leq D$, where r is the radial distance from the center of the particle and D is the cell radius), are determined by the PB equation:

$$\frac{1}{r}\frac{\partial^2 r\psi(r)}{\partial r^2} = 4\pi l_{\text{B}} n_0 \exp(\psi(r)) \tag{16}$$

where $n(r) = n_0 \exp(\psi(r))$ is the local number density of (negatively charged) counterions, $\psi(r) \equiv e\Psi(r)/k_BT$ is the dimensionless electrostatic potential, and n_0 is a constant that depends on the calibration of the electrostatic potential. If we set $\psi(D) = 0$, then n_0 is the concentration of counterions at the cell edge, $r = D$. Equation (16) has to be complemented by two boundary conditions:

$$\left(\frac{\partial \psi(r)}{\partial r}\right)_D = 0 \qquad \left(\frac{\partial \psi(r)}{\partial r}\right)_{R_c} = -\frac{l_B Q}{R_c^2} \tag{17}$$

where the former reflects the electroneutrality of the cell as a whole.

If the value of the electrostatic potential at the particle surface is low, $\psi(R_c) \approx l_B Q/R_c \ll 1$, the electrostatic potential at $r \geq R_c$ is even lower and the linearized form of the PB equation, often referred to as the Debye Hückel (DH) approximation:

$$\frac{1}{r}\frac{\partial^2 r\psi(r)}{\partial r^2} = \kappa^2(1 + \psi(r)) \tag{18}$$

can be safely applied in the whole cell volume, $R_c \leq r \leq D$. Equation (18), together with the boundary conditions (17), correctly describe the electrostatic potential $\psi(r)$ and the number density of counterions $n(r) = \frac{\kappa^2(1+\psi(r))}{4\pi l_B}$ in the whole cell. Here $\kappa^2 = 4\pi l_B n(D)$ and the value of κ has to be found from the boundary conditions (and the calibration of the potential, $\psi(D) = 0$), together with the solution of (18). In the dilute regime, $D \gg R_c$, one finds that $\kappa^2 \approx 2l_B Q/D^3$. The counterion concentration at $r = D$, which determines the osmotic pressure in the solution, equals $n(D) = \kappa^2/4\pi l_B$. Hence, $n(D) \approx Q/2\pi D^3$, and the counterions are distributed fairly uniformly throughout the cell (the concentration of counterions near the edge of the cell is close to the average concentration). This is what one also expects from the Boltzmann law, $n(r) = n(D)\exp(\psi(r))$, with a low value of the reduced potential ($\psi(r) \leq 1$) throughout the cell.

If the particle is strongly charged, so that it creates a large surface potential $\psi(R_c) = l_B Q/R_c \gg 1$, the DH approximation cannot be used in the proximity of the surface. However, the DH approximation can still be safely applied far away from the particle surface (close to the cell boundary $r = D$, where the potential is reduced to values $\psi(r) \leq 1$). At this point, we come to the concept of charge renormalization: when $l_B Q/R_c \gg 1$ and the electrostatic potential at the surface of the charged particle is high, $\psi(R_c) \gg 1$, a certain number of counterions become localized ("condensed") in the vicinity of the surface and this reduces the apparent surface potential down to a level $\psi \sim 1$. The last condition determines the number of uncondensed (osmotically active) counterions as $Q^* \sim R_c/l_B$. In the range $r \gg R_c$, where the potential is sufficiently reduced, one can again apply the DH approximation and describe the radial distribution of uncondensed counterions using the DH equation presented above, wherein the actual charge of the particle Q is replaced by a renormalized charge $Q^* \sim R_c/l_B$. Similarly to the case for weakly charged particles, the osmotically active counterions are distributed fairly uniformly in the range $R_c \ll r \leq D$, so that their concentration at $r = D$ and the osmotic pressure

coincide (with the accuracy of a numerical factor on the order of unity) with their average concentration in the cell $\sim Q^*/D^3$. We note that, even though one can never unambiguously distinguish between condensed and uncondensed counterions, the value of Q^* has a clear physical meaning (as it appears in the DH solution), which properly matches the exact (PB) distribution of the potential (and of the counterion density) in the peripheral and intermediate regions of the cell.

In contrast to a solid charged colloid, a branched polyion can accommodate a large number of counterions in its interior volume. The analogy between the charge renormalization in a solution of hard-core colloids and the counterion localization in a star-like PE or a colloidal PE brush was first pointed out by Pincus [26]. Because counterions retain translational degrees of freedom in the intramolecular volume of a polyion, they exert an osmotic pressure to the volume of the corona. Hence, the polyion swells due to the "entrapped" counterions. The uncompensated charge within the star corona with radius R equals the number of released (osmotically active) counterions and is given by $Q^* \sim R/l_B$. The electrostatic potential drops to a value $\psi(R) \cong 1$ at the edge of the corona, and the distribution of counterions in the exterior space, $R \leq r \leq D$, is fairly uniform.

3.4 *Effects of Concentration and Interactions in Star Polyelectrolyte Solutions*

The cell model enables one to describe the effects of polymer concentration, which manifest themselves in a salt-free solution of PEs, even in the dilute regime. Here, the solution is modeled as an array of spherical Wigner–Seitz cells, each comprising one branched polyion with its counterions. The radius D of each cell equals half the average distance between polyions in the solution. As has been demonstrated in [29], PE stars exhibit a pronounced contraction upon an increase in polymer concentration (a decrease in D) in dilute solutions, $D \geq R$. This effect is caused by the progressive re-partitioning of counterions from the inter- to the intramolecular space. An increase in polymer concentration makes the counterion distribution more uniform, leading thereby to a decrease in the uncompensated charge of the star Q^* and a corresponding decrease of the electrostatic potential ψ at the edge of the star.

A decrease in the size, R, of a PE star as a function of polymer concentration is most pronounced for polyions with a relatively small number of branches p. As discussed above, in this case the counterions are distributed most uniformly between intra- and intermolecular space. Therefore, an increase in the average concentration of counterions in the solution leads to a proportional increase in their concentration in the intramolecular volume of these branched polyions. In contrast to this, stars that have many arms have a modest response to an increase in the PE concentration. This is because at any (arbitrarily small) solution concentration, only a small fraction of the counterions is found in the intermolecular space. This behavior of PE stars should be contrasted with that of neutral star polymers. In the latter case, screening of the intramolecular excluded-volume repulsion, and the contraction of

star-branched polymers upon the increase in star concentration, occurs only in the semidilute regime, i.e., when the average polymer concentration in the solution exceeds the intramolecular concentration in an isolated star [24].

The repulsive forces acting between the PE stars in salt-free solutions are of long-range character. Analogous to the crystalline ordering of charged colloids [36], PE stars might organize in a three-dimensional periodic lattice. This long-ranged ordering is governed by the Coulomb repulsion between star polyions. The magnitude of this repulsion is controlled by the effective (uncompensated) charge Q^* of the star. The formation of a periodic supramolecular structure is only expected in a certain range of PE concentrations. The lower concentration limit is specified by the condition that the energy of Coulomb repulsion between neighboring polyions becomes on the order of $k_B T$. An upper concentration limit arises due to the enhanced screening of interstar Coulomb repulsion upon an increase in the solution concentration [27].

Probing forces between PE stars in a solution is a challenging experimental problem. However, advances in the technique of optical tweezers now allow direct measurement of repulsive forces between brushes of DNA [94, 95] and synthetic PE chains [96, 97] grafted onto colloidal particles of submicrometer size.

The MD simulation study of the interaction between PE stars in a salt-free solution has been performed in [39]. The simulation results were fitted using a simplified analytical equation for repulsive force, which arises due to the decrease in translational entropy of counterions entrapped in overlapping star coronae. In this model, the repulsion starts at distances between star centers smaller than $2R$, where R is the unperturbed size of an individual star. A similar approach has been applied in [40] to describe repulsion between colloidal PE brushes.

The repulsive force between colloidal PE brushes in a salt-free solution can be calculated within the PB–Derjaguin approximation (Zhulina and Borisov, unpublished data) without pre-assumptions about the spatial distribution of counterions. This can be done on the basis of an exact solution of the PB problem for a planar PE brush in a salt-free solution [98]. Application of the Derjaguin approximation implies that size of the particle, $R_c + H$ (where H is the thickness of corona of colloidal PE brush) exceeds by far the characteristic thickness of ionic atmosphere. Then, the total force $\mathcal{F}$ acting between spherical PE brushes is given by:

$$\mathcal{F}(d) = 2\pi(R_c + d)\int_d^\infty \Pi(D)dD \tag{19}$$

Here, $2d$ is the smallest distance between the surfaces of spherical core particles, whereas $\Pi(D)$ is the disjoining pressure between two planar PE brushes (with the same grafting density, degree of ionization, and degree of polymerization of grafted PEs) at separation $2D$ between the grafting surfaces. Note that the latter expression is applicable in the range of interparticle separations $2d \ll 2(R_c + H)$. The disjoining pressure, $\Pi(D)$, as well as the brush thickness, $H(D)$, were calculated in [98].

Analysis shows that the force versus separation profile, calculated from (19), exhibits a different shape depending on the surface charge density due to grafted

polyions. If the surface of the particle is decorated by the "osmotic" PE brush, i.e., $H(d=\infty) \gg \Lambda$, where $\Lambda = s/2\pi l_B \alpha N$ and s is the grafting area per chain, then the majority of counterions are localized inside the brush and:

$$\frac{\mathcal{F}}{k_B T R} \approx \begin{cases} \pi^2/4 l_B d, & H(d=\infty) \ll d \ll R_c \\ (\Lambda l_B)^{-1} \ln\left[H(d=\infty)/d\right], & d \ll H(d=\infty) \end{cases} \tag{20}$$

In the opposite case of a relatively sparse PE brush, $H(d=\infty) \ll \Lambda$, the thickness of ionic atmosphere is $\cong \Lambda$, and most of counterions are retained in the proximity of the particle outside the brush. Under these conditions, the force–distance profile is given by:

$$\frac{\mathcal{F}}{k_B T R} \approx \begin{cases} \pi^2/4 l_B d, & \Lambda \ll d \ll R_c \\ (\Lambda l_B)^{-1} \ln\left(\Lambda/d\right), & d \ll \Lambda \end{cases} \tag{21}$$

Comparison of (20) and (21) shows that at large separations, the force $\mathcal{F}$ decays as $\sim 1/d$, irrespective of the charge density created on the particle surface by the PE brush. In the case of a sparse PE brush with fairly uniform distribution of counterions within the layer of thickness $\cong \Lambda$, the crossover to logarithmic force decay occurs smoothly at $d \cong \Lambda$. By contrast, in the case of the osmotic brush with strongly inhomogenous distribution of counterions (most of them trapped inside the brush), the repulsive force $\mathcal{F}$ sharply increases at $d \cong H(\infty)$, i.e., when the coronas of colloidal PE brushes approach close contact.

We emphasize that the Derjaguin approximation leads to a qualitatively different physical picture for interacting colloidal PE brushes compared to that in [40]. According to [40], the repulsion between spherical colloids decorated by PE brushes starts when the opposing brushes "touch" each other, i.e., at distance $2d = 2H$ between colloid surfaces, where $H = H(d=\infty)$ is the thickness of the unperturbed PE brush. According to the PB–Derjaguin approximation, the interaction between counterion atmospheres perturbs the chain conformations in PE brushes prior to their overlap. The grafted chains in the gap between core particles locally contract, and the PE brush becomes asymmetric upon the approach of colloids. That is, the brush thickness $H(d)$ is minimal at the smallest distance, $2d$, between surfaces of core particles, and gradually increases up to $H(d=\infty)$ outside the gap between colloids. In contrast to the model in [40], PE colloidal brushes remain separated by a layer of water, containing mobile ions, for a range of distances $2d < 2H(\infty)$, until the thermal fluctuations of terminal arm segments close the gap between PE brushes.

It is expected that a similar physical picture also holds for interacting PE stars. At distances between core domains $2d \geq 2R$, the star coronae would start to contract due to the overlap of ionic atmospheres. As a result, the stars would become asymmetric and remain separated by a water layer in a range of distances $2d < 2R$. The long-range interactions due to the overlap of ionic atmospheres are essential for PE stars with a moderate number of arms (typical for experimental systems), and at low ionic strength in the solution [27].

4 Localization of Counterions in Salt-Free Solutions of Branched Polyelectrolytes: Effect of the Polyion Topology

The localization of counterions in the intramolecular volume is a common feature manifested in dilute salt-free solutions of branched polyions of different topologies, including dendritic (star-burst), randomly (hyper)branched PEs, PE molecular brushes, etc. The physical reason for this phenomena is the same as outlined for PE stars: a strongly charged, branched, macroion creates a high electrostatic potential, which attracts counterions and retains them in the intramolecular volume, in spite of a significant loss in the translational entropy. The effect is most pronounced in a dilute solution, where the concentration of counterions in the bulk is extremely low.

Remarkably, linear PEs of arbitrary large N cannot induce a similar effect. This is because both the charge, αNe, and the size, $R \cong aN(\alpha^2 l_B/a)^{1/3}$, of a stretched polyion in a dilute salt-free solution, scale proportionally to N [91, 92], so that their ratio remains $\sim \alpha^{1/3} \leq 1$. Note that we do not discuss here the effect of Manning condensation, which occurs when the distance between two neighboring charges along the chain is smaller than l_B. A detailed discussion of this case can be found in [93].

A theoretical analysis of the effect of counterion localization in a dilute solution of weakly charged branched polyions of different topologies [31–33] and ionic microgels [34, 35], was performed on the basis of a cell model, similar to that used here for a star-like PE. The elastic term in the free energy that accounts for the conformational entropy of a uniformly swollen branched macromolecule, has to be specified depending on the polyion topology. The shape of the cell might also be modified. For example, in the case of a molecular PE brush, a cylindrical instead of spherical cell should be used.

Similarly to the case of a quenched star-like PE, two regimes of ion distribution were distinguished. A fairly uniform distribution of "free" counterions is found at low degree of branching, whereas a strong localization of counterions in the intramolecular volume is expected for a high degree of branching of the polyion. In the latter case only a minor fraction of the counterions is released to the exterior volume of the cell.

We recall that for a star-like PE, the transition from the regime of a barely charged polyion, to the osmotic regime, occurs at a characteristic number of branches, $p \cong \alpha^{-1/2}(l_B/a)^{-1}$. The latter depends on the combination of the parameters $\alpha(l_B/a)^2$, and is independent of the length N of an arm. Below we briefly summarize the results obtained for branched polyions of different topologies.

4.1 Ionic Dendrimers (Star-Burst Polyelectrolytes)

The conformations of charged (regular) star-burst polymers (flexible ionic dendrimers), were analyzed theoretically in [33]. Referring to Fig. 4a, relevant architectural parameters for a star-burst polymer are the number of generations,

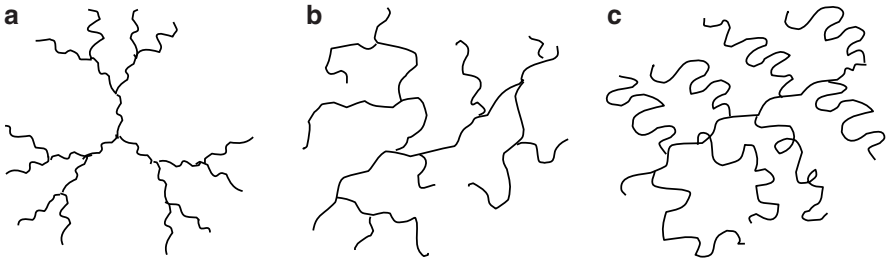

Fig. 4 Branched polyions of different topologies: star-burst (**a**), randomly branched or hyper-branched (**b**), molecular brush (**c**)

g, and the length of a spacer, n. If each branching point has a functionality 2, then the total degree of polymerization is $N = 3n(2^g - 1)$, where $g = 1, 2, \ldots$. In a uniformly swollen dendrimer, all the spacers are extended in the radial direction. The conformational free energy of a dendrimer, with a distance R between the center of the molecule and the ends of the last generation spacers, is given by [33]:

$$F_{\text{conf}}/k_{\text{B}}T \cong \frac{2R^2(g)}{na^2}\left(1 - \frac{4}{3}g^{-2}\right)^{-1} \tag{22}$$

where a force balance condition was used in each branching point. Substituting this equation into the free energy of the cell model, (7), leads to the following expression for the size of ionic dendrimer:

$$R_{\text{dendr}} \cong \begin{cases} aN^{2/3}(\alpha^2 l_{\text{B}}/a)^{1/3}n^{1/3}, & N/n \ll (\alpha(l_{\text{B}}/a)^2)^{-1} \\ aN^{1/2}\alpha^{1/2}n^{1/2}, & N/n \gg (\alpha(l_{\text{B}}/a)^2)^{-1} \end{cases} \tag{23}$$

Hence, counterion localization occurs when the number of generations in the star-burst polymer, $g \approx \log_2(N/n)$, reaches some characteristic value, which is controlled by the same combination of the parameters, $\alpha^{-1}(l_{\text{B}}/a)^{-2}$, as for a PE star. Note that this combination is independent of the spacer length, n.

4.2 Randomly Branched Polyelectrolytes and Charged Fractals

A randomly branched PE was modeled in [31, 32], as a branched tree (without loops) formed by N bi- and trifunctional monomers, cf. Fig. 4b. The average number of trifunctional monomers (branching points) is $\sim N/n$, so that the average number of monomers in a spacer, connecting two neighboring branching points, is n. The condition of $N/n \gg 1$ corresponds to the limit of strong branching, whereas at low branching probability, $N/n \cong 1$, the linear chain behavior is recovered. Here we insist that the average spacer contains a large number of monomers, $n \gg 1$. The opposite limit of $n \cong 1$ corresponds to a hyper-branched polymer. The conformational

entropy losses due to the uniform swelling of a randomly branched polymer, up to the size R, can be accounted for as [99, 100]:

$$F_{\mathrm{conf}}/k_{\mathrm{B}}T \cong \frac{R^2}{(Nn)^{1/2}a^2} \tag{24}$$

where $R_{\mathrm{ideal}} \cong a(Nn)^{1/4}$ is the unperturbed, Gaussian, size of an ideal, randomly branched polymer [101]. Balancing the entropic elastic force with the intramolecular Coulomb repulsions and/or the osmotic pressure of counterions leads to:

$$R_{\mathrm{random}} \cong \begin{cases} aN^{5/6}(\alpha^2 l_{\mathrm{B}}/a)^{1/3}n^{1/6}, & N/n \ll (\alpha(l_{\mathrm{B}}/a)^2)^{-2} \\ aN^{3/4}\alpha^{1/2}n^{1/4}, & N/n \gg (\alpha(l_{\mathrm{B}}/a)^2)^{-2} \end{cases} \tag{25}$$

An interesting feature of (25) is the fractal dimension, specifying how the mass $\sim N$ of a randomly branched PE depends on its size R. For small clusters that release many counterions into the bulk solution, $d_{\mathrm{f}} = 6/5$, whereas for large (osmotic) clusters, $d_{\mathrm{f}} = 4/3$. Again, the counterion localization threshold is set by the increase in the electrostatic potential, $\cong l_{\mathrm{B}}Q/R$ which grows upon an increase in N as $\sim N^{1/6}$ in the regime of free counterions (small clusters). Another remarkable feature of (25) is, that the counterion condensation threshold occurs when the number of branching points N/n reaches the characteristic value $\cong \alpha^{-2}(l_{\mathrm{B}}/a)^{-4}$, which again is independent of the spacer length n.

These results have been generalized further in [31], for charged polymeric fractals with arbitrary connectivity characterized by spectral dimension, d_{s}, (the latter relates the longest path in the fractal, $R_{\max} \cong aN^{1/d_{\mathrm{s}}}$, to its mass $\sim N$) and arbitrary fractal dimension d_{f} (in the absence of ionic charges) in d-dimensional space. For ideal (Gaussian) fractals $d_{\mathrm{f}} = 2d_{\mathrm{s}}/(2-d_{\mathrm{s}})$. For charged fractals:

$$R_{\mathrm{fractal}} \cong \begin{cases} aN^{\frac{2d_{\mathrm{f}}-d_{\mathrm{s}}}{d_{\mathrm{s}}d_{\mathrm{f}}+(d-2)(d_{\mathrm{f}}-d_{\mathrm{s}})}}(\alpha^2 l_{\mathrm{B}}/a)^{\frac{d_{\mathrm{f}}-d_{\mathrm{s}}}{d_{\mathrm{s}}d_{\mathrm{f}}+(d-2)(d_{\mathrm{f}}-d_{\mathrm{s}})}}, & N \ll N^* \\ aN^{1/d_{\mathrm{s}}}\alpha^{\frac{d_{\mathrm{f}}-d_{\mathrm{s}}}{d_{\mathrm{s}}d_{\mathrm{f}}}}, & N \gg N^* \end{cases} \tag{26}$$

Here, the threshold value for the number of monomers, corresponding to the onset of charge renormalization, is specified as:

$$N^* \cong \alpha^{\frac{d_{\mathrm{s}}d_{\mathrm{f}}-(d-2)(d_{\mathrm{f}}-d_{\mathrm{s}})}{d_{\mathrm{f}}(d-2-d_{\mathrm{s}})}}(l_{\mathrm{B}}/a)^{\frac{d_{\mathrm{s}}}{(d-2-d_{\mathrm{s}})}} \tag{27}$$

As follows from (26) charge renormalization effects occur only when $d < d_{\mathrm{s}} + 2$.

4.3 Polyelectrolyte Cylindrical (Molecular) Brushes

Molecular brushes are polymers composed of a long main chain (backbone), onto which side chains (grafts) are attached at regular intervals. See Fig. 4c for a graphic illustration. The graft-copolymers are classified as molecular brushes, provided the

number of monomer units in a graft, n, exceeds that in a spacer (the segment of the backbone between two neighboring grafts), m. A steric or electrostatic repulsion between the grafts (referred to as crowding), leads to their extension in the radial direction. The crowding of grafts induces an axial tension in the backbone, which, in turn, also gets stretched. Locally, the molecular brush acquires a cylindrical symmetry on a length scale that is characterized by an apparent (or induced) persistence length [102–107]. The latter is comparable to, or exceeds, the brush thickness, which is controlled by the radial extension of the side chains, R.

The box-like model considers a molecular PE brush with the backbone extended along the axis of an (infinitely long) cylindrical cell of radius D, wherein the end segments of the grafts are localized at a distance $R \ll D$ from the axis of the cell. The cell contains counterions who compensate the net charge of the brush. This model enables one to analyze the local conformational properties and the distribution of the counterions in a dilute salt-free solution of molecular PE brushes. The Coulomb interactions (calculated per graft) can be presented as:

$$F_{\text{Coulomb}}/k_{\text{B}}T = -l_{\text{B}}q^{*}\ln(R/a)\varphi(R/D) \tag{28}$$

where q^{*} is the number of counterions, per unit length along the cell axis, that is released from the brush, and $\varphi(x)$ is a rational function of x. The conformational free energy (per graft) includes the contributions from both a spacer, extended up to length h, and a graft, extended up to length R:

$$F_{\text{conf}}/k_{\text{B}}T = \frac{3}{2a^{2}}\left(\frac{R^{2}}{n}+\frac{h^{2}}{m}\right) \tag{29}$$

The Gaussian elasticity of the grafts and spacers could be modified to account for the local swelling effects [102]. Finally, the translational entropy of the counterions is accounted for as:

$$F_{\text{ions}}/k_{\text{B}}T = h(q-q^{*})\ln c_{\text{ions}}^{(\text{in})} + hq^{*}\ln c_{\text{ions}}^{(\text{out})} \tag{30}$$

where $q \approx \alpha n/h$. The minimization of this free energy with respect to R, h and q^{*}, provides the thickness of a molecular PE brush:

$$R \cong \begin{cases} an^{7/6}(\alpha^{2}l_{\text{B}}/a)^{1/3}m^{-1/6}, & n/m \ll (\alpha(l_{\text{B}}/a)^{2})^{-1} \\ an\alpha^{1/2}, & n/m \gg (\alpha(l_{\text{B}}/a)^{2})^{-1} \end{cases} \tag{31}$$

The characteristic branching parameter (grafting density), $n/m \cong \alpha^{-1}(l_{\text{B}}/a)^{-2}$, specifies the onset of counterion localization inside the molecular brush. Note that in the osmotic regime, the spacers get fully extended, $h \sim m$. It is therefore not surprising, that the counterion localization in a cylindrical molecular brush coincides (in scaling terms) with the Manning condensation threshold [25] for a charged cylinder, $ql_{\text{B}} \cong 1$.

Molecular brushes composed of biopolymers, are typically more complex than their synthetic analogs. They may comprise different types of biomacromolecules, and involve self-assembly mechanisms. For example, in aggrecanes [108] and

mucins [109], polysaccharide side chains are densely grafted ($m \cong 1$) to an unfolded core protein with intergraft distance $h \cong am$. In cylindrical assemblies of neuronal proteins (neurofilaments, or NFs), a rigid core comprises numerous coiled-coil domains of constituent proteins. The flexible side arms of three different lengths (referred to as projections) emanate from the core at a distance $h = 2 - 3$ nm between the grafts, and form a corona with thickness $R \simeq 40$ nm [110]. The large persistence length $\simeq 450$ nm [110] insures local cylindrical symmetry and the nematic ordering of NFs in hydrogels [111, 112]. Variations in the environmental conditions (pH, solution salinity, etc.) affect the conformations of protein projections, but do not change intergraft distance h. The brushes (coronae) of heavily charged ($\alpha \simeq 0.1 - 0.2$) projections prevent close approach of neurofilaments, presumably due to the electrostatic repulsions between the grafts [113].

Box-like model highlights generic PE features of a neurofilament brush [114]. It specifies the onset of osmotic regime, and rationalizes the increase in brush thickness, R, upon progressive protein phosphorylation (an increase in α). An advanced SF-SCF numerical modeling highlights the respective roles of different NF proteins in coronal organization and the conformational re-arrangements triggered by the phosphorylation [115–119]. It demonstrates an approximately parabolic profile for the electrostatic potential $\psi(r)$ in the NF brush proximal region, occupied by the shortest projections. A parabolic shape of $\psi(r)$ was theoretically predicted for a planar PE brush [98], and is also found to be a reasonable approximation for a cylindrical PE brush [114].

5 Localization of Counterions in a Salt-Free Solution of Polyelectrolyte Stars: Numerical Results

Theoretical predictions concerning the localization of counterions in salt-free solutions of star-branched PEs have provoked a number of studies on this effect using different numerical simulation techniques. Although MD [40–42] and MC [38] simulations have given a qualitative proof of a clearly inhomogeneous distribution of the counterions (whose concentration differs between the interior and exterior of the star), the numerical SCF modeling has allowed a more systematic and quantitative study of the effect of macroion branching on the degree of counterion localization. The latter technique was used to explore the transition from the charged star regime to the osmotic regime, and to quantify the fraction of released (osmotically active) counterions as a function of number of branches in a star polymer.

5.1 Molecular Dynamics and Monte Carlo Simulations

MC [38] and MD simulations [39–42] provided an unambiguous proof of the preferential localization of counterions in the intramolecular volume of a star polymer.

Furthermore, in the case of a sufficiently high linear charge density in the branches ($\alpha \cong 1$), the simulations indicated a strong correlation in the angular distribution of the counterions and the position of an arm. That is, a certain fraction of the counterions that are entrapped inside a star polymer have restricted translational freedom and can be envisioned as "condensed" on the branches. This effect is analogous to the classical Manning condensation of counterions on a strongly charged linear PE [25]. A typical snapshot of the PE star with its counterions is shown in a paper of Jusufi et al. (see figure 2b of [84]), wherein three possible states of the counterions can be visually distinguished: (a) condensed around the arms, (b) possessing translational freedom but localized in the intrastar volume, and (c) released into the solution.

Mean field theories that implement a spherically symmetric distributions of counterions assume that the (effective) charge density on the star branches is below the Manning condensation threshold. In this limit, one can neglect the angular correlations between the positions of the arms of the star and those of its counterions.

5.2 Self-Consistent Field Poisson–Boltzmann Theory

A quantitative analysis of counterion localization in a salt-free solution of star-like PEs is described in [29, 37]. Radial distributions for both the electrostatic potential and the density of counterions were obtained by a numerical solution of the corresponding PB problem within a cell model. The conformational degrees of freedom of the branches of a central star were accounted for within the SF-SCF method [120]. Due to the computational efficiency, the SF-SCF framework allows for a systematic study of a many-armed star with sufficiently long arms in a large cell. The range of the parameters that could be covered by the SF-SCF method exceeds that of contemporary MD and MC simulations.

The PB equation was solved at low concentrations of 1:1 electrolyte using the discretization scheme in a spherical coordinate system with a PE star in the center. The characteristic length of a lattice site is set equal to the monomer length, which is fixed to $a = 0.5\,\text{nm}$ (close to the Bjerrum length $l_B \approx 0.7\,\text{nm}$ in water). The corresponding conversion factor for the volume fraction of salt, φ_s, to the corresponding molar concentration obeys $c_s \approx 12.9\varphi_s\,\text{M}$. All lengths are normalized with the length a of a lattice site. The default value of $N = 200$ was taken for the arm length. The number of arms per star p was varied in the range 20–50. The first segment of each arm was restricted to be near the center of the coordinate system. PE stars with a fixed (quenched) fraction of charged monomers $0.2 \leq \alpha \leq 1.0$ were considered. Because the monomer size a is slightly smaller than l_B, the effect of Manning condensation becomes relevant for $\alpha \approx 1$. It can, however, be safely neglected at lower values of the fractional charge α. The outer radius of the cell D was taken as large enough to minimize finite cell size effects. All nearest-neighbor interactions, except for the excluded volume effects, were neglected (athermal solvent conditions). Further details of the SF-SCF method can be found in [37].

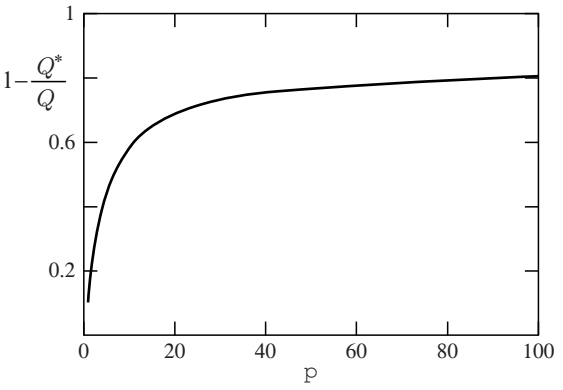

Fig. 5 Fraction of counterions localized inside the star (at $r < R$) as a function of the number of branches, p, under theta-solvent conditions; $N = 200$, $\alpha = 0.2$, $D = 150$, volume fraction of salt in the bulk solution $\varphi_s^b = 10^{-7}$; Q total bare charge of the star, Q^* uncompensated charge

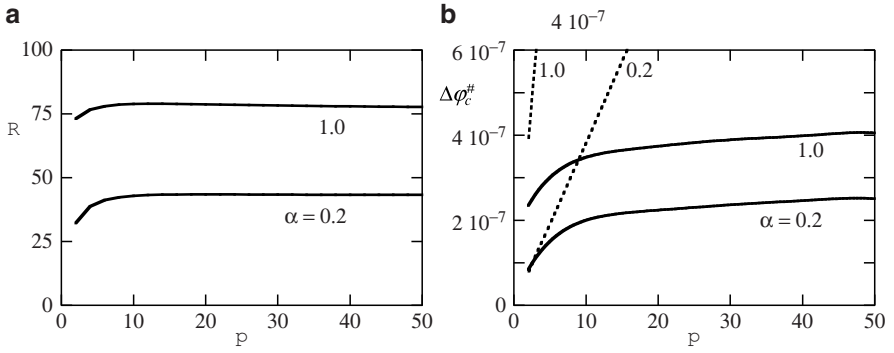

Fig. 6 (**a**) The first moment of the radial end-point distribution, R, as a function of the number of arms p in the PE stars; $N = 100$, $D = 500$, and α as indicated. (**b**) The corresponding excess density (volume fraction) of ions at the system boundary. The *dotted lines* are the expected results when all counterions of the PE star are distributed homogeneously in the system

In Fig. 5, the average fraction of counterions, $1 - Q^*/Q$, that are localized inside the star (i.e., at $r \leq R$, where the star size R is introduced as a first moment of the radial distribution of arm terminal segments) is presented as a function of the number of branches, p.

In Fig. 6, the star size R and the excess concentration of counterions at the outer cell boundary, $r = D$, are presented as a function of the number of arms, p, for different values of α (shown by solid lines). Dotted lines in Fig. 6b, indicate the corresponding expectations for uniform distribution of the cell counterions. An increase in the number of arms in each star implies an increase in the number of charged monomers $Q = p\alpha N$, and in the corresponding number of mobile counterions in the cell. Figures 6 and 7 clearly demonstrate a transition from a "barely charged" to an "osmotic" star behavior upon the increase in p. At a relatively small number of arms, the star size and the concentration of counterions at the outer cell boundary grow as a function of p. The latter is approximately proportional to p and is close to the average counterion concentration in the cell. This proves that ions

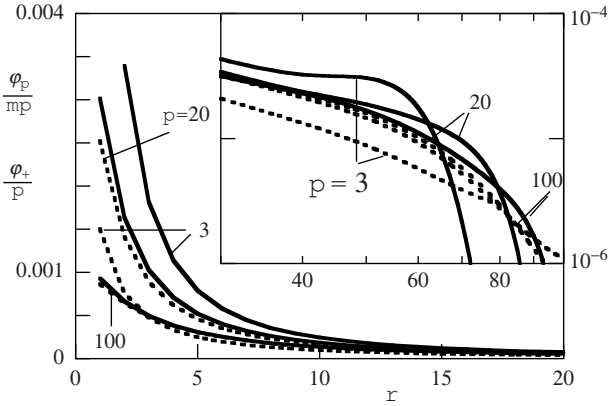

Fig. 7 Radial volume fraction profile, normalized per arm and by the distance between charges $m = \alpha^{-1}$, i.e., $\varphi_p(r)/pm$ (*solid lines*), and the radial counterion density profile, normalized by the number of arms, i.e. φ_+/p (*dotted lines*), for stars with different numbers of branches p as indicated, under theta-solvent conditions; $N = 200$, $\alpha = 0.2$, $D = 150$, $\varphi_s^b = 10^{-7}$. *Inset*: the same curves in log–log coordinates

are distributed fairly uniformly between interior and exterior volumes of a star with a small number of branches. By contrast, the size of a many-armed star becomes almost independent of p (in line with the expectation in the osmotic regime). Here, the concentration of osmotically active counterions grows weakly as a function of p, and is much smaller than the average concentration of counterions in the cell. (The latter grows proportionally to p, as shown by the dotted lines in Fig. 6b).

In Fig. 7, the radial density profiles of charged monomers and of counterions (normalized for one branch) are shown for stars with different numbers of arms, p (in a salt-free system). For small p, the distribution of counterions is fairly uniform, whereas that for the stars with a large number of arms both distributions almost coincide.

Based on the SF-SCF results, we may give a quantitative estimate for the characteristic number of branches at which a PE star enters the osmotic regime. As follows from Fig. 7, for the experimentally relevant range of $\alpha \leq 1$, this number is of the order of unity. That is, a star polymer with ~ 10 arms efficiently retains its counterions and is reliably found in the osmotic regime.

6 Localization of Counterions in a Salt-Free Solution of Star-Like Polyelectrolytes: Experimental Results

The effect of counterion confinement in star-branched polyions manifests itself most directly in osmotic pressure measurements. The osmotic pressure is a colligative property of the solution and is determined by the (number) density of mobile particles. In a dilute salt-free PE solution, the osmotic pressure is controlled by the number density of osmotically active counterions, because their number is much

larger than the number of polyions. The degree of confinement of counterions is quantified by the osmotic coefficient ϕ, which is the ratio of the measured osmotic pressure to the net average concentration of counterions in the solution.

As discussed in Sect. 3.3, the distribution of the counterions outside the corona of the PE star is fairly uniform. Therefore, the osmotic coefficient ϕ approximately equals the ratio Q^*/Q.

The osmotic coefficient ϕ has been measured both in solutions of strongly dissociating poly[2-(methacryloyloxy)ethyl]-trimethylammonium iodide (PMETAI) [48], and weakly dissociating PAA [43] star polymers.

Figure 8a presents the osmotic coefficients measured in solutions of PMETAI and PAA stars with 18 and 21 arms, respectively, as a function of the polymer

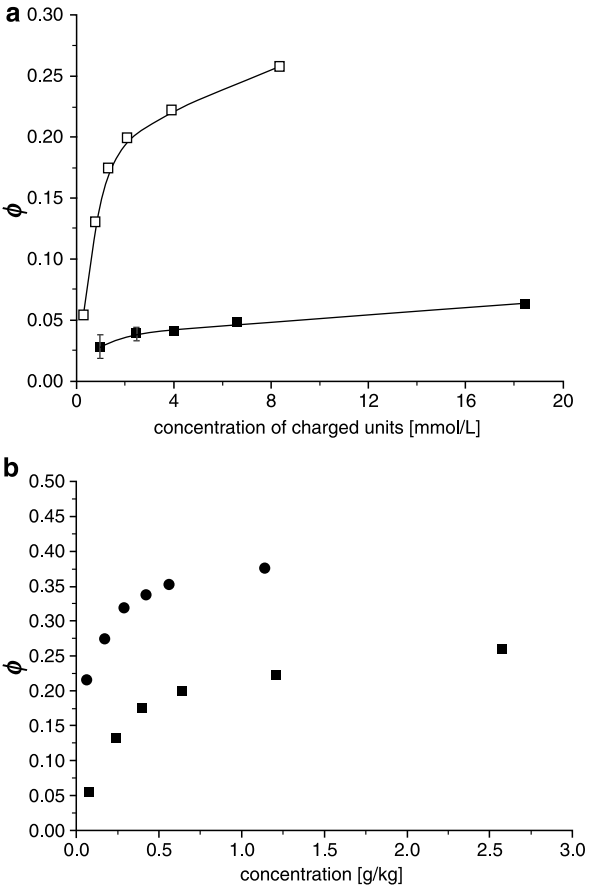

Fig. 8 Osmotic coefficients in solutions of (**a**) PMETAI stars with 18 arms, each comprising 170 monomer units (*closed squares*) and PAA stars with 21 arms, each comprising 100 monomer units, degree of neutralization $\alpha = 0.24$ (*open squares*), and (**b**) PAA stars with 8 (*circles*) and 21 (*squares*) arms, each arm comprises 100 monomer units, degree of neutralization $\alpha = 0.25$, as a function of polymer concentration

concentration. The experimental curves demonstrate a weak increase in the osmotic coefficient as a function of polymer concentration. However, in both cases, the osmotic coefficient is significantly lower than unity and its magnitude is close to that obtained in [37] on the basis of SF-SCF calculations. This unambiguously proves the reduced osmotic activity of counterions. This reduction can be rationalized by their confinement in the intramolecular volume.

Clearly, for pH-sensitive PAA stars, the osmotic coefficient depends on the degree of ionization α, which is controlled by the pH in the solution. Under these conditions, the lower charge of a PAA star as compared with that of a fully ionized ($\alpha \cong 1$) PMETAI star, leads to a lower degree of localization of counterions and, thereby, to a larger value of the osmotic coefficient ϕ.

In Fig. 8b, we show the osmotic coefficients for PAA stars that differ with respect to the numbers of arms at the given degree of neutralization. In accordance with theoretical predictions, the osmotic coefficient ϕ decreases (i.e., the degree of localization of counterions increases) upon an increase in the number of arms, p, in the star. Note that in the case of star polymers with relatively small number of arms, the osmotic coefficient is significantly larger (by two orders of magnitude) than that measured previously in the solutions of colloidal PE brushes [44, 45].

7 Effects of Ionic Strength and pH on the Polyelectrolyte Star Conformation

From the summary of the theoretical results presented above, it follows that the intramolecular volume of a star-branched PE, with a sufficiently large number of arms, is essentially electroneutral. That is, the bare charge of a star polymer is neutralized by mobile counterions. These counterions are predominantly retained inside the macroion volume, even if the star is immersed in a dilute salt-free solution. Moreover, if the "intrinsic" Debye length associated with the intramolecular concentration of entrapped counterions, $r_{\mathrm{D}}^{(\mathrm{in})} \cong (l_{\mathrm{B}} p\alpha N/R^3)^{-1/2}$, is used as an upper estimate for the intramolecular electrostatic screening length, one finds that in the osmotic PE star, $p \gg \alpha^{-1/2}(l_{\mathrm{B}}/a)^{-1}$, the electrostatic interactions are screened at distances much smaller than the star size R.

Therefore, a detailed analysis of the conformations of many-armed star-like PEs may take place within the so-called local electroneutrality approximation (LEA). The latter also allows for an equilibrium of the ionization of the macroion, hence also covering the pH-responsive (annealing) star-like PEs.

As long as monovalent salt ions are added to the solution, the total ion concentration:

$$\Phi_{\mathrm{ion}} \equiv \sum_j c_{bj} \tag{32}$$

determines the ionic strength, and the Debye screening length in the bulk of the solution is:

$$r_{\mathrm{D}} = (4\pi l_{\mathrm{B}} \Phi_{\mathrm{ion}})^{-1/2} \tag{33}$$

(The summation in (32) is performed over all ion species, including H^+ and OH^- ions).

The effect of salt on the conformations of a many-arm (osmotic) PE star becomes important when the salt-controlled bulk Debye screening length, given by (33), becomes smaller than the intrinsic screening length, $r_{\mathrm{D}}^{(\mathrm{in})}$, in a salt-free osmotic PE star. This is also true, equivalently, when the concentration of added salt exceeds the intramolecular concentration of counterions in the osmotic star. Clearly, the local electroneutrality in this case is ensured, and the LEA is applicable for analysis of the PE star conformations on a length scale larger than r_{D}.

The opposite limiting case of a PE star with a small number $p \ll \alpha^{-1/2}(l_{\mathrm{B}}/a)^{-1}$ of arms in a salt-free solution was considered in [121]. In the latter case, the counterions can be disregarded and the Poisson equation allowed for an exact numerical solution for the polymer density profile, which confirmed the uniform stretching of the arms in the interior region of the star. The LEA may be applied for analysis of conformations of stars with a small number of arms in salt-added solution, provided the bulk Debye length r_{D} is smaller than the overall size of the star [28].

7.1 The Mean-Spherical Equal Arm Stretching Approximation: General Formalism

To analyze the effects of ionic strength and pH of the solution on the conformations of PE stars, we switch from the "canonical" cell model (where the number of ions was fixed) to the "partially open" ensemble. In the latter model, (a) one central star polymer occupies a spherical volume within radius R, and (b) the chemical potentials of all mobile ions are set equal to those in the bulk of the solution (infinite reservoir).

The concentrations c_{bj} (or, equivalently, the chemical potentials) of all the mobile ions are assumed to be constant in bulk solution. Therefore, the relevant free energy of the corona is the Gibbs free energy.

If all the star branches are assumed to be equally stretched (i.e., all the ends of the arms are localized at the edge of the star), the free energy of a star polymer can be presented as:

$$F = p\frac{3k_{\mathrm{B}}T}{2a^2}\int_0^R \left(\frac{\mathrm{d}r}{\mathrm{d}n}\right)\mathrm{d}r + 4\pi\int_0^R f_{\mathrm{int}}\{c_{\mathrm{p}}(r)\}r^2\mathrm{d}r \tag{34}$$

Here, the first term accounts for the conformational entropy losses in non-uniformly extended branches that exhibit the Gaussian elasticity [122], whereas the second term is the interaction contribution to the free energy. The local chain extension $(\mathrm{d}r/\mathrm{d}n)$ at distance r from the center is related to the local concentration of monomers, $c_{\mathrm{p}}(r)$, as:

$$c_{\mathrm{p}}(r) = \frac{p}{4\pi r^2}\frac{\mathrm{d}n}{\mathrm{d}r} \tag{35}$$

Then, the free energy, (34), can be presented as:

$$F = 4\pi \int_0^R f\{c_p(r), r\} r^2 \mathrm{d}r \tag{36}$$

where:

$$f\{c_p(r), r\} = \frac{3k_B T p^2}{32\pi^2 a^2 r^4 c_p(r)} + f_{int}\{c_p(r)\} \tag{37}$$

is the total density of the free energy in a star polymer.

The term $f_{int}\{c_p(r)\}$ accounts for the short-ranged (excluded volume) interactions between monomers $f_{ev}\{c_p(r)\}$ and for the ionic contribution $f_{ion}\{c_p(r)\}$:

$$f_{int}\{c_p(r)\} = f_{ev}\{c_p(r)\} + f_{ion}\{c_p(r)\} \tag{38}$$

where:

$$f_{ev}\{c_p(r)\}/k_B T = \upsilon c_p^2(r) + w c_p^3(r) + \ldots \tag{39}$$

The expressions for the ionic contribution to the free energy density, $f_{ion}\{c_p(r)\}$, are derived within the LEA in the Appendix, both for quenched and annealing PE coronas.

The polymer density profile, $c_p(r)$, and the radius of the star, R, are determined from the minimization of the free energy, (36), while taking the conservation of the number of monomer units, (2) into account as a constraint. This leads to:

$$\frac{\delta}{\delta c_p(r)} f\{c_p(r), r\} = \lambda \tag{40}$$

Here λ is a Lagrange multiplier that is coupled to the constraint that the total number of the monomer units, (2) is conserved. The constant λ coincides with the exchange chemical potential of the monomer, which is constant throughout the star. The equilibrium value of R is obtained by a minimization of the free energy with respect to R, which is equivalent to the condition that the differential osmotic pressure vanishes at the edge of the corona $r = R$:

$$\Delta\Pi(r = D) \equiv \left(c_p(r) \frac{\delta}{\delta c_p(r)} f\{c_p(r), r\} - f\{c_p(r), r\} \right)_{r=R} = 0 \tag{41}$$

In a simplified model, which generalizes the Daoud–Cotton approach [21], the condition of a local balance between the elastic tension in the extended branches and the excess osmotic pressure due to (repulsive) monomer–monomer interactions:

$$c_p(r) \frac{\delta}{\delta c_p(r)} f\{c_p(r), r\} - f\{c_p(r), r\} = 0 \tag{42}$$

is implemented at all distances r from the center of the polyion. This "quasi-planar" approach generalizes the blob model that was described in Sect. 2. Clearly, the normalization condition for the polymer density profile (2) also has to be satisfied.

When (42) is used in the derivation of the polymer density profile, the profile appears independent of the degree of polymerization N of the arms. The degree of polymerization N only determines the cut-off distance for the profile via the normalization condition, (2). This implies that the local conformations of the arms at any distance $r < R$ are independent of N. In particular, the elastic tension in the chains at any distance $r < R$ does not depend on the overall degree of polymerization of the chains.

Alternatively, implementing (40) and (41) leads to a quite different picture for the star structure. Here, the elastic tension in the arms is determined by the local monomer–monomer repulsion only at the edge of the corona, $r = R$. At $r < R$ the arms are stretched more strongly, due to an excess pulling force exerted by the terminal parts of the arms. Therefore, the polymer density profile $c_p(r,N,R)$ and the chemical potential $\lambda(N,R)$ depend explicitly on N (or the star size R) [123].

7.2 Density Profiles

Closed analytical expressions for the polymer density profiles $c_p(r)$ can be obtained only in certain limiting cases (asymptotic regimes), when the free energy density can be presented as a power law function of the polymer concentration, $f_{int}\{c_p(r)\} \sim c_p^{\gamma}(r)$. The density profiles have the simplest form when they are presented in reduced variables, r/R and $c_p(r)/c_p(R)$.

A simplified quasi-planar approach predicts a power law decay of the density profile for any value of γ and at any distance r:

$$c_p(r)/c_p(R) \approx (R/r)^{\frac{4}{\gamma+1}} \tag{43}$$

A more accurate theory predicts a different functional form for the density profile that depends on the value of γ. The polymer concentration, $c_p(r)$, can be approximated by a power law function only in the central region of the corona.

For a neutral star, $\gamma = 2$ or 3 in a good or a theta-solvent, respectively. The same exponent, $\gamma = 2$, is found for a PE star in a concentrated salt solution, see (60). The latter is not surprising, because at a high salt concentration, the electrostatic repulsion between charged monomers is partially screened and the monomer–monomer interactions are described via binary short-range repulsion.

By simultaneously solving (40) and (41), one gets for the polymer density profile:

$$c_p(r)/c_p(R) \approx \left(\frac{\gamma-1}{2\gamma}\right)^{\frac{1}{\gamma+1}} (R/r)^{\frac{4}{\gamma+1}} \tag{44}$$

Hence, the power law dependencies $c_p(r) \sim r^{-4/3}$ and $c_p(r) \sim r^{-1}$, derived above for neutral star polymers under good and theta-solvent conditions, are recovered, but the numerical prefactor is smaller than in quasi-planar model, (43).

In the case of a quenched PE star in a low salt solution (osmotic regime), $\gamma = 1$ and:

$$c_p(r)/c_p(R) \approx (R/r)^2 \{2\ln[c_p(r)/c_p(R)]\}^{-1/2} \tag{45}$$

We, therefore, find a logarithmic correction to the polymer density profile predicted earlier, $c_p(r) \sim r^{-2}$, which corresponds to a uniform radial stretching of the arms.

Finally, the density profile found for an annealing PE star in the low salt regime, $\gamma = 1/2$, is:

$$c_p(r)/c_p(R) \approx (R/r)^2/3^{1/2} \tag{46}$$

Here, the density profile decays as $c_p(r) \sim r^{-2}$, which corresponds to a uniform stretching of the arms in interior region of an annealing PE star. Note that this result differs from that obtained in a simplified quasi-planar model ($c_p(r) \sim r^{-8/3}$). The latter predicts an increase in the local stretching of the arms as a function of distance r from the star center. Remarkably, in spite of the difference in the polymer density distributions specified by the two models, the overall size R of the star macromolecule obeys the same power law dependence [123]. One can therefore use either of the two approaches, or even a box-like cell model, to get the power law dependencies for the star size R.

We emphasize that in both models discussed here, the free ends of the branches are fixed at the external boundary of the corona. Relaxation of this constraint is possible in the numerical SCF model of Scheutjens and Fleer. It is therefore instructive to compare the predictions of the analytical theory to the more accurate results obtained by means of the numerical SF-SCF computations.

In Figs. 9 and 10a, the polymer volume fraction profiles are presented in double logarithmic (log–log) coordinates for both quenched and annealing stars with

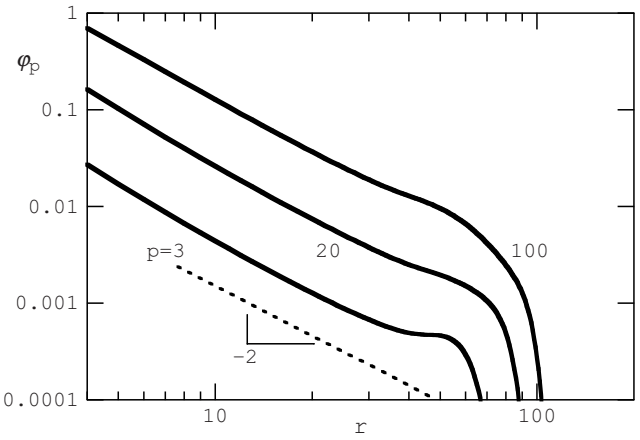

Fig. 9 Radial volume fraction profile $\varphi_p(r)$ (in log–log coordinates) for quenched PE stars with different numbers of branches p; theta-solvent conditions; $N = 200$, $\alpha = 0.2$, $D = 150$, $\varphi_s^b = 10^{-7}$. The *dotted line* indicates the slope -2, corresponding to a uniform extension of the branches

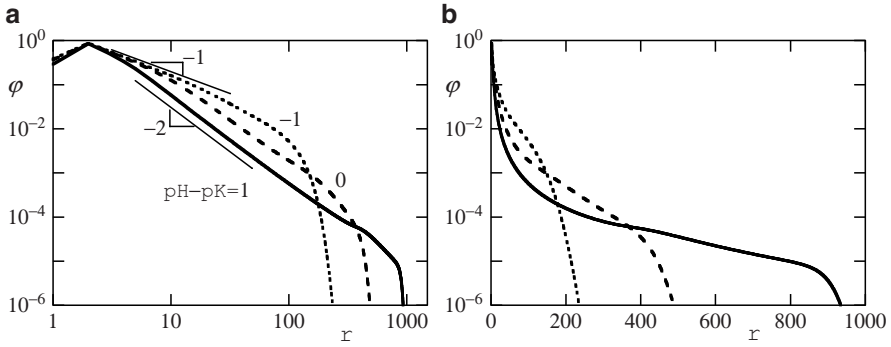

Fig. 10 Radial polymer volume fraction profiles $\varphi_p(r)$ for three values of the difference between pH and pK_a: -1, 0 and 1 under theta-conditions; $N = 4000$ $p = 20$, $\varphi_s^b = 10^{-7}$. (**a**) Double logarithmic (log–log) coordinates; the slopes -2 and -1 are indicated. (**b**) Semilogarithmic coordinates

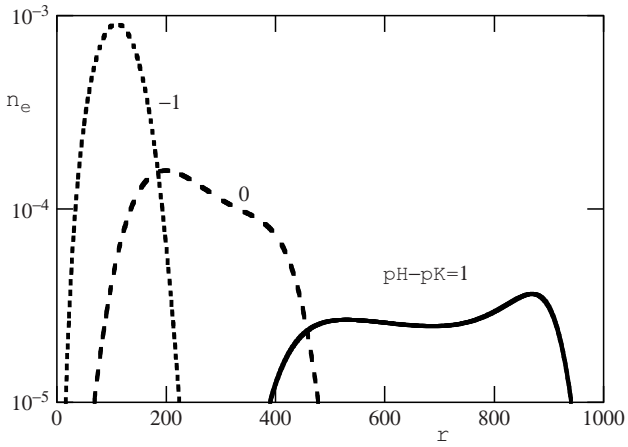

Fig. 11 Radial distribution of end segments $n_e(r)$ for three values of the difference between pH and pK_a: -1, 0 and 1 under theta-conditions; $N = 4000$ $p = 20$, $\varphi_s^b = 10^{-7}$; semilogarithmic coordinates

different numbers of arms, p, respectively. A power law decay with slope -2 is clearly seen in central regions of both quenched and annealing PE stars. This corresponds to a uniform stretching of the arms. In Fig. 10b, the volume fraction profiles for annealing PE stars are presented in semilogarithmic coordinates. These prove that there is an exponential decay of the polymer density in the peripheral region of the star corona.

In Fig. 11, the radial distribution of the end segments in an annealing PE star, with different number p of arms, is shown for a range of pH values. A "dead zone", i.e., a region close to the center of the star where free ends are depleted, is visible. The end-point distribution is clearly bimodal for $pH \geq pK_a$, when the star corona

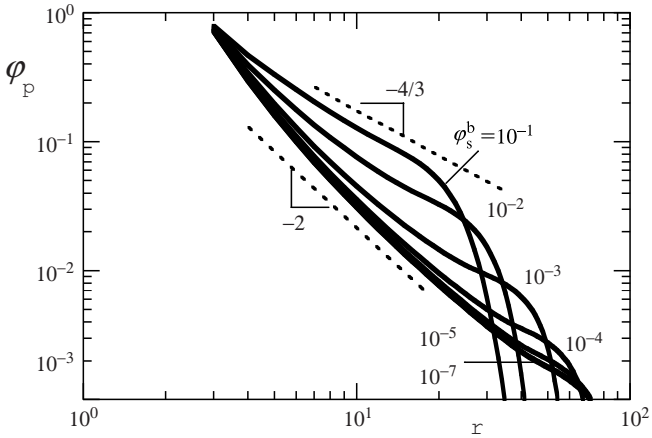

Fig. 12 Radial volume fraction profile of polymer segments $\varphi_p(r)$ in log–log coordinates, of a quenched PE star with $p = 20$ branches under theta-conditions; $N = 200$, $\alpha = 0.2$, $D = 300$, for various ionic strength conditions (φ_s^b) as indicated. *The dotted line* with the slope -2 corresponding to a uniform extension of the branches

is moderately ionized. Obviously, the two peaks in the distribution of chain ends correspond to two populations of the arms: the stronger ionized ones constitute the distal maximum in the distribution, whereas the weaker ionized ones are less stretched and contribute to the proximal maximum.

In Fig. 12, similar segment density profiles are presented for quenched PE stars with a given number of arms, $p = 20$, and for several salt concentrations, in log–log coordinates. Clearly, in the central region a power law regime is recovered. At low salt concentration, the slope -2 corresponds to the uniform stretching of the arms. Upon an increase in salt concentration, this slope is progressively changed to $-4/3$, corresponding to the salt-dominated regime.

The results of the SF-SCF calculations indicate that fluctuations in the extension of individual branches lead to a wide peripheral distribution of the free ends. Similarly to a neutral star polymer [124], the corona of a PE star consists of two regions. In the internal region, the arms are stretched fairly equally, and the decay of the polymer density is described by a power law function. This is in good agreement with findings of the analytical theory, which uses the assumption of equal stretching of the arms. At the periphery of a star polymer, the curvature effects are less important. Here, the corona can be structurally mimicked by a quasi-planar PE brush [98]: the free ends are distributed throughout the peripheral region with a well-pronounced maximum. For a quenched PE star polymer, the self-consistent electrostatic potential can be approximated by a parabolic function, whereas the number density profile of monomers has either a Gaussian (in a salt-free case) or a parabolic (in a salt-added case) shape, followed by an exponential decay at the tail of the distribution. The latter arises due to the fluctuations of non-stretched terminal segments of the arms.

7.3 Star Size and Degree of Ionization

In the context of the LEA, the size R of a PE star can be obtained by integrating the polymer density profile, $c_p(r)$, according to (2). In the limiting cases, when the density profiles are described by a power law function of distance from the star center, (44)–(46), the exact numerical pre-factors in the scaling expressions can be specified for the star size. Remarkably, if the simplified quasi-planar approach is applied, the star size is systematically underestimated. As mentioned above, this is due to a neglected additional pulling force exerted on the central regions of the star by the terminal segments of its arms. The difference between the results obtained by the two different approaches is marginal in the case of nonionic star polymers, whose conformations are governed by short-ranged repulsive intramolecular interactions, or for PE stars at high salt concentration. However, it becomes significant for PE stars at low salt concentrations, particularly for weakly dissociating (pH-sensitive) PE stars.

Quenched Polyelectrolyte Star

For the dimensions of a quenched PE star in a salt-free osmotic regime, one recovers the scaling dependence, (14), obtained earlier on the basis of a box-like model.

An increase in concentration Φ_{ion} of added salt ions, leads to the penetration of salt ions into the star interior and a decrease in the differential osmotic pressure. When the concentration of added ions sufficiently exceeds the average concentration of counterions in the osmotic star, the polyion is found in the so-called salt-dominated regime. Here, the differential osmotic pressure of ions is equivalent to that created by binary monomer–monomer interactions with an effective second viral coefficient $\upsilon_{eff} = \alpha^2/2\Phi_{ion}$. As a result, one recovers the same scaling dependence for the size of a PE star as that found for neutral star polymer under good solvent conditions, (4), with replacement $\upsilon \to \upsilon_{eff}$:

$$R \cong aN^{3/5}p^{1/5}(\alpha^2/a^3\Phi_{ion})^{1/5} \tag{47}$$

We, therefore, find that the PE star size, R, in the salt-dominated regime decreases as $\Phi_{ion}^{-1/5}$, upon an increase in salt concentration. Note that the same scaling dependence is obtained when the electrostatic repulsions between the charged monomers are accounted for through the screened Coulomb binary interaction potential, $u(r)/k_BT = l_B r^{-1}\exp(-r/r_D)$. A further increase in Φ_{ion} leads to an additional decrease in υ_{eff}. When υ_{eff} becomes on the order of the bare virial coefficient υ, the star size R approaches that of a neutral star, (4). Therefore, the size R of a quenched PE star demonstrates a plateau at low salt concentrations (in the osmotic regime), decreases in the salt-dominated regime as $R \sim \Phi_{ion}^{-1/5}$, and approaches a second plateau at high salt concentrations (in the quasi-neutral regime), as schematically illustrated in Fig. 13.

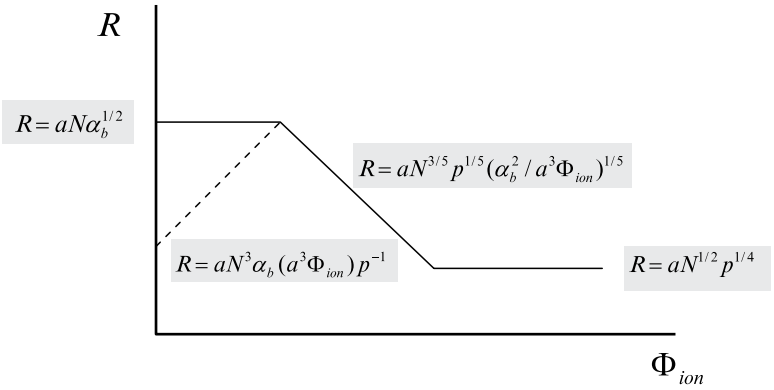

Fig. 13 Evolution of the size (radius R) of quenched and annealing PE stars as a function of salt concentration Φ_{ion}. See text for details

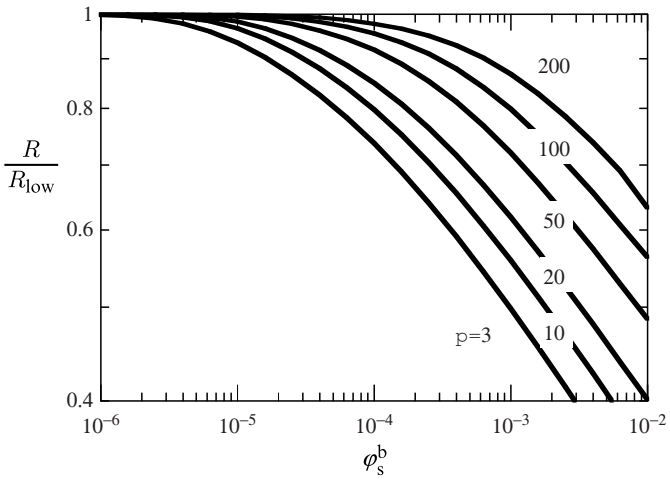

Fig. 14 Quenched PE star size R as a function of the volume fraction of salt in the bulk φ_s^b (in log–log coordinates) for stars with different number of branches p as indicated, under theta-conditions; $N = 200$, $\alpha = 0.2$, $D = 150$. The size is normalized with respect to the limiting value at low ionic strength conditions R_{low}

In Fig. 14, the overall size of a quenched PE star is plotted as a function of salt concentration for different values of p (in log–log coordinates). In accordance with the analytical predictions, the plateau at low salt is followed by a decrease in the star size with a slope of -0.2.

The salt-controlled behavior of PE coronae of kinetically frozen star-like micelles was examined experimentally [52, 58]. A good correspondence between the theoretical $(-1/5)$ and the observed (-0.18 in [52], and -0.2 in [58]) values of the exponent was found.

A more refined scaling model, developed recently in [93], introduces the concept of a screening length $r_B < r_D$ to specify the PE star behavior in the salt-dominated regime. According to [125], r_B governs the screening of the electrostatic interactions in a semidilute PE solution with added salt. A smaller value of $r_B = r_D \alpha^{1/6}$, with respect to the salt-controlled Debye length, r_D, is due to a more effective screening by charged polymer segments than by single ions. However, such modification leads to a rather moderate revision compared to the osmotic model described above. In particular, it predicts the appearance of a very narrow subregime, wherein $R \sim \Phi_{ion}^{-1/2}$. This dependence is expected in the middle of the salt-dominated regime (wherein $R \sim \Phi_{ion}^{-1/5}$), but up to now it has not been detected experimentally.

Annealing Star Polyelectrolyte

In contrast to the monotonous decrease in R expected for quenched PE stars upon an increase in salt concentration, an annealing PE star polymer demonstrates more sophisticated behavior. As discussed above, the ionization equilibrium in a strongly branched polyion is coupled to the local concentration of hydrogen ions in its interior (local pH) according to the mass action law (5). The local pH (computed using the local proton concentration) in an anionic star is always lower than the "buffered" pH in the solution, and the degree of ionization α of a monomer in a polyion interior is, therefore, lower than that in the bulk of the solution. Therefore, the degree of ionization of the star branches could be tuned by variations either in the ionic strength or in the pH of the solution. As a result, an annealing PE star might demonstrate a non-monotonous variation of its dimensions as a function of salt concentration Φ_{ion}.

The LEA gives, for the average degree of ionization α of a highly branched PE star:

$$\alpha \cong \begin{cases} \alpha_b^2 a^6 N^4 p^{-2} \Phi_{ion}^2, & \alpha_b c_p / \Phi_{ion} \gg 1 \\ \alpha_b, & \alpha_b c_p / \Phi_{ion} \ll 1 \end{cases} \tag{48}$$

where α_b is the degree of ionization of a monomer in the bulk solution at given pH. Hence, at low salt concentration Φ_{ion}, the average degree of ionization of monomers in a star polymer is a decreasing function of the number of arms, p, and increases upon an increase in Φ_{ion}, asymptotically approaching (from below) the value of α_b.

In Fig. 15, the average degree of ionization versus the bulk pH is plotted for weak polyacid stars with different numbers of arms. A progressive shift of the curves towards larger pH values upon an increase in p is clearly noticeable. Correspondingly, at low salt concentrations, the size $R \cong aN\alpha^{1/2}$ of an annealing PE star is given by:

$$R \cong a^4 N^3 p^{-1} \alpha_b \Phi_{ion}, \qquad \alpha_b c_p / \Phi_{ion} \gg 1 \tag{49}$$

The theory, therefore, predicts a linear increase in the size of an annealing PE star polymer at relatively low salt concentration (in the osmotic regime), as shown by the dashed line in Fig. 13. When salt is added, salt ions substitute protons in the interior of the polyion and thereby increase the local pH. As a result, the ionization of the branches increases, and the PE star swells upon an initial increase in Φ_{ion}.

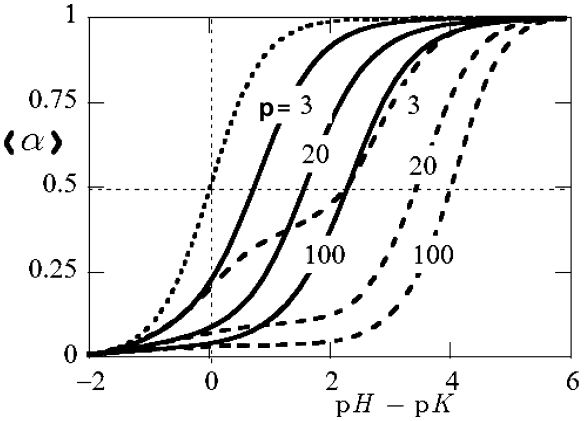

Fig. 15 Average fraction of dissociated groups $\langle\alpha\rangle$ as a function of the difference between pH of the solution and the pK_a value of the weak acidic groups. The number of branches (p) is indicated; theta-conditions and $N = 200$ The ionic strength is $\varphi_s^b = 10^{-5}$ ($c_s = 10^{-4}$ M) (*solid lines*) and $\varphi_s^b = 10^{-7}$ ($c_s = 10^{-6}$ M) (*dashed lines*)

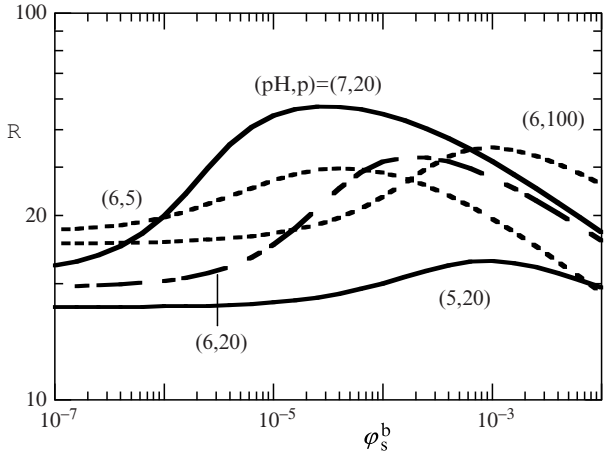

Fig. 16 Size of an annealing PE star R as a function of the ionic strength for $N = 200$, $D = 500$, $m = 5$, p$K_a = 6$ under theta-conditions. The pH is 6 or 7, and the number of branches p is 5, 20, or 100 as indicated

When the local (interior) pH approaches the bulk pH, $\alpha \cong \alpha_b$ and the size of a swollen polyion reaches its maximum, $R \cong aN\alpha_b^{1/2}$. After this point, the behavior of quenched and annealing PE star polymers becomes similar: both decrease their size R upon a further increase in Φ_{ion} as $R \sim \Phi_{ion}^{-1/5}$, following (47), and approach the quasi-neutral plateau at high salt conditions (as schematically shown in Fig. 13).

In Fig. 16, the average size R of an annealing PE star (specified as the first moment of the end segment distribution) is plotted as a function of the salt concentration, $\Phi_{ion} \sim \varphi_s^b$, for different values of the bulk pH. A maximum is observed for $pH \leq pK_a$.

At low salt concentration, however, the degree of ionization α of an annealing PE star might become so low that a star macroion releases a noticeable fraction of its counterions into the surrounding solution. As a result, the increase in local pH promotes ionization of the branches. The released counterions become more strongly attracted to the macroion and eventually condense back into its interior. Therefore, under low salt conditions, an annealing branched macroion stays at the threshold of ion release, $Q = \alpha pN \cong R/l_B$. The ion localization condition, $\alpha pN \cong R/l_B$, together with the intrastar osmotic balance condition, $R \cong a\alpha^{1/2}N$, set the scaling dependence for the star size in this so-called annealing charged regime [28]:

$$R \cong \frac{a^2 N}{l_B p} \tag{50}$$

The crossover between (49) and (50) specifies the boundary between the annealing osmotic and the annealing charged regimes as $a^2 l_B \alpha_b N^2 \Phi_{ion} \approx a^2 l_B K_a N^2 \Phi_{ion}/c_{bH+} \simeq 1$.

Remarkably, in both annealing charged and annealing osmotic regimes, (49) and (50) predict a decrease in the star size as a function of the number of branches p. The reason for this is a decrease in the average degree of ionization of the arms upon an increase in the intramolecular density of the monomers. However, the strong dependence, $R \sim p^{-1}$, predicted by (49) and (50) is hardly observable in real or numerical experiments because of a corresponding increase of the non-electrostatic (excluded-volume) intramolecular repulsion.

Various scaling regimes of quenched and annealing PE star polymers are summarized in the diagram of states given in Fig. 17. For an annealing star, in addition to the annealing osmotic and annealing charged regimes (where the star size R is given by (49) and (50), respectively), one finds the regime of a charged star (13), the salt-dominated regime (47), and the regime of a neutral star (3). The latter is specified in Fig. 17 for theta-solvent conditions, $\upsilon = 0$. Remarkably, in the charged annealing regime, the size R of a star polymer does not exhibit a power law dependence on Φ_{ion}. This might explain why, in contrast to planar brushes, the spherically curved weak PE colloidal brushes do not demonstrate a distinct increase in R upon an increase in Φ_{ion} [45]. Note that, in a planar geometry, the scaling theory predicts a salt-induced increase in brush thickness, $H \sim \Phi_{ion}^{1/3}$, for both the annealing osmotic and the annealing charged regimes [126]. Whereas the general theoretical trends predicted for the annealing planar and quasi-planar brushes were confirmed in a number of experimental studies [45, 127–133], a comprehensive test of annealing star-like spherical brushes remains a challenging problem. The width of the osmotic annealing regime is rather limited (see diagram in Fig. 17), and a proper choice of the relevant parameters (p, N, and pH) is of crucial importance for detecting the $R \sim \Phi_{ion}$ dependence, (49).

The coupling between the ionization of an annealing polyion and its conformation is expected for other branched macroions as well. Recently, this effect was unambiguously demonstrated for thermoresponsive spherical star-like micelles of diblock copolymers with a polybasic (PDMAEMA) corona [134]. Due to the

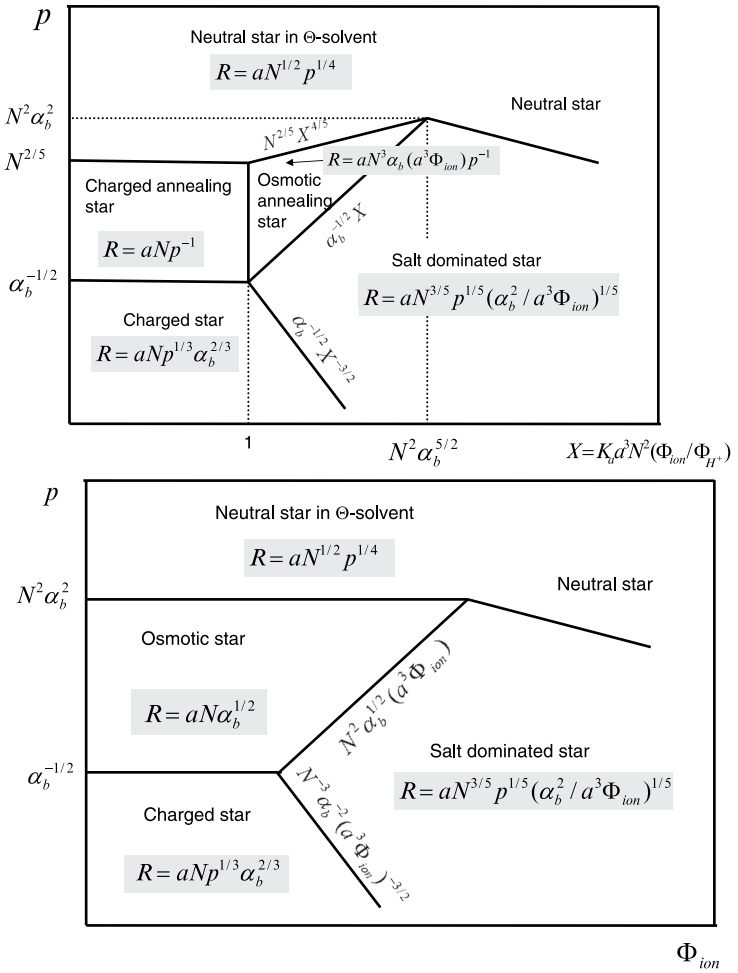

Fig. 17 Diagram of states of annealing (**a**) and quenched (**b**) PE stars. The ratio l_B/a is set to unity. See text for details

connection between the conformations of coronal chains and the ionization of their segments, variations in the temperature and pH could cause large micelles with a quasi-neutral corona to reversibly abruptly rearrange into small micelles with a highly charged corona.

7.4 Annealing Star Polyelectrolytes: Titration Curves

To experimentally monitor the ionization of weak PE stars, one can measure the variation of the pH in the solution of PE stars upon adding strong acid or strong base.

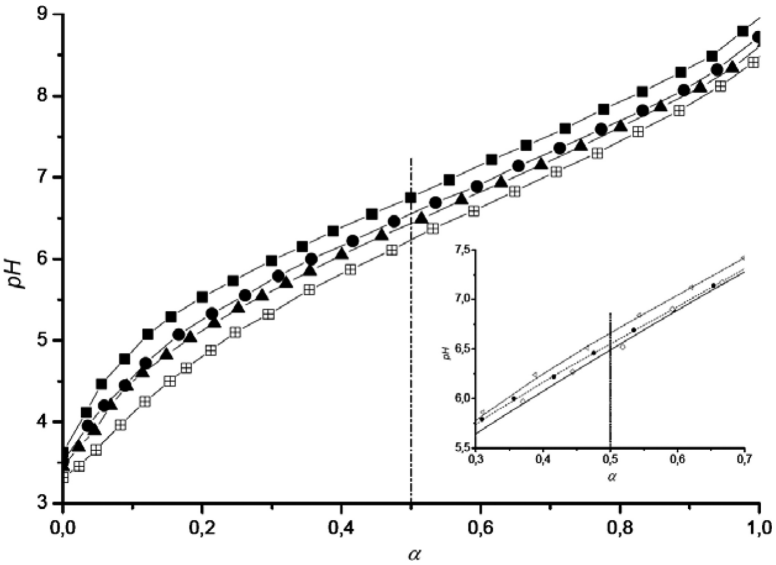

Fig. 18 Potentiometric titration curves for PAA stars: $(PAA_{100})_{21}$ (*closed squares*), $(PAA_{100})_8$ (*closed circles*), $(PAA_{100})_5$ (*closed triangles*), and linear PAA_{100} (*open squares*). *Inset* is the cutout of $(PAA_{75})_8$ (*open triangles*), $(PAA_{160})_8$ (*open diamonds*), and $(PAA_{100})_8$ (*closed circles*) [43]. Reprinted by permission of Wiley-VCH

The degree of neutralization of the PE macroion can be calculated from the added amount of acid or base in relation to the detected pH. The apparent pK_a (or pK_b) values can be found from the pH that corresponds to the degree of neutralization of $\alpha = 0.5$.

A solution of PAA stars was titrated by adding a concentrated NaOH solution, giving a titration curve [43]. Figure 18 shows the obtained result for pH as a function of the degree of neutralization, $\alpha = [Na^+]/[COOH]$, where [COOH] is the total concentration of carboxyl and carboxylate groups of the stars and $[Na^+]$ is equal to the amount of added NaOH. It is clearly seen that the titration curves are systematically shifted toward larger pH values when the number of arms (at constant arm length) is increased. This result is in accordance with (48). Thus, the apparent pK_a increases as a function of the number or arms, as predicted by theory: the larger the number of arms, the higher the excess electrostatic potential inside the star and the smaller is the degree of ionization of the arms.

7.5 Effect of Counterion Valency

As discussed in the previous section, the addition of monovalent salt to a solution of PE stars leads to a screening of the intramolecular Coulomb repulsion and a subsequent decrease of the differential osmotic pressure. For quenched PE stars, this results in a monotonic decrease in the star size, most pronounced in the

salt-dominated regime. For pH-sensitive PE stars, the promotion of ionization due to replacement of H^+ (or OH^-) counterions by salt ions dominates under low salt conditions and, as a result, the star swells upon an addition of salt (cf. osmotic annealing regime in Fig. 17). This swelling is followed by a decrease in the star size, R, at higher salt concentrations (salt-dominated regime in Fig. 17). Both trends are strongly affected by the valency of the counterions.

The effect of counterion valency on the swelling behavior of planar and colloidal PE brushes was theoretically studied in [135–137]. In the case of a counterion with a valency of Z ($Z = 1$, 2 and 3 for, e.g., Na^+, Ca^{2+} and Al^{3+} ions, respectively), the Donnan equilibrium is formulated as:

$$c_{Z+}/c_{bZ+} = (c_{j^+}/c_{bj^+})^Z = (c_{bj^-}/c_{j^-})^Z = \exp(-Ze\Delta\Psi/k_BT) \tag{51}$$

where c_{Z+} and c_{bZ+} are the concentrations of the Z-valent ions inside and outside the star, and $c_{j^\pm}$ and $c_{bj^\pm}$ are the concentrations of monovalent ions (including H^+ and OH^- ions) inside the star volume and in the bulk of the solution, respectively. In experiments, the ratio $c_{bZ}/Z\sum_{j^+} c_{bj^+} \equiv \zeta$ and the total concentration of monovalent salt co-ions, $\sum_{j^-} c_{bj^-} \equiv \Phi_s/2$, are often used as control parameters.

By combining (51) with the local electroneutrality condition, $\sum_{j^-} c_{j^-} + \alpha c_p = \sum_{j^+} c_{j^+} + Zc_{Z+}$, one finds an equation for the excess (Donnan) potential inside the star and for the differential osmotic pressure. This differential osmotic pressure has to be balanced with the elastic force of entropic origin that is linked to the extension of the branches to give the equilibrium size of the star polymer.

It can be shown that the addition of trace amounts of Z-ions to the solution leads to a rapid substitution of monovalent counterion in the star corona by Z-ions. This is due to their stronger attraction to the oppositely charged PE star polymer. Since a smaller number of Z-ions is needed to ensure the electroneutrality of the star interior, an increase in ζ (i.e., in relative amount of Z-ions in the bulk of the solution) leads to a rapid decrease in the osmotic pressure inside the corona and, consequently, to a de-swelling of the PE star. This effect, of replacing monovalent counterions by multivalent ones is most pronounced at low salt concentrations (in the osmotic regime), where:

$$R \cong aN\left(\frac{\alpha}{Z}\right)^{1/2} \tag{52}$$

and, thus, $R_{Z=1}/R_Z \cong Z^{1/2}$. By contrast, in the salt-dominated regime, the differential osmotic pressure and the star size, R, are controlled by the ionic strength in the solution via r_D. That is, $R \cong aN^{3/5}p^{1/5}\upsilon_{eff}^{1/5}$, where:

$$\upsilon_{eff} = 2\pi\alpha^2 l_B r_D^2 = \frac{\alpha^2}{\Phi_s}\cdot\frac{1+Z^2\zeta}{2+Z^2\zeta+Z^3\zeta} \tag{53}$$

Thus, the replacement of monovalent counterions by multivalent ones (at constant and high bulk concentration of monovalent salt co-ions), results in a contraction of the star macroion by a factor of $R_{Z=1}/R_Z \cong Z^{1/5}$.

The effect of multivalent counterions has been studied experimentally for colloidal PE brushes in [137]. Remarkably, the magnitude of the observed collapse described in [137] exceeds the decrease in R predicted on the basis of osmotic balance arguments (52). A similar trend was also found for planar PE brushes in the presence of multivalent ions [132, 138]. At least two additional effects might be responsible for this behavior. Firstly, a correlational attraction in the star corona, due to Z-ions, may serve as a co-driving force of the star collapse. Secondly, multivalent counterions might bind specifically (adsorb) to the star branches, thereby reducing their effective charge density. Under these conditions, the Donnan equilibrium should be supplemented by a Langmuir-like balance [139] between the counterions that are adsorbed onto the branches and the mobile ones in the star interior. Finally, one has to keep in mind that the replacement of monovalent counterions by multivalent ones reduces the maximal charge density on the arms corresponding to the Manning condensation threshold.

For an annealing star polyion, the degree of ionization, α, becomes a function of the counterion valence, Z, and of the Z-ion bulk concentration, c_{bZ}, due to a progressive substitution of the monovalent counterion (H^+ for a polyacid) by Z-ions and the corresponding increase in local pH inside the star. Implementation of the Donnan rule (51), together with the mass action law (5) and the osmotic balance (52), provides a scaling dependence for the star size:

$$R \cong a\alpha_{\mathrm{b}}^{Z/(2Z-1)} N^{(2Z+1)/(2Z-1)} \left(\frac{Zc_{bZ}}{p}\right)^{1/(2Z-1)} \tag{54}$$

where the exponents depend on the counterion valency, $Z \geq 1$. Remarkably, under low salt conditions the substitution of monovalent counterions by multivalent ones leads to a weaker swelling of the star corona (as a function of the added salt concentration). In the salt-dominated regime, multivalent counterions provide a stronger screening of the electrostatic interactions (smaller value of the Debye length, r_{D}) for both quenched and annealing polyions.

8 Collapse of a Polyelectrolyte Star in Poor Solvent

Triggered by a decrease in the solvent strength, isolated nonionic star polymers suffer a collapse transition. The theory of the collapse transition has been developed in [140, 141]. This theory predicts a progressive deswelling (collapse) of the star polymer as a function of decreasing solvent strength. The onset of the collapse transition, which corresponds, e.g., to a vanishing second virial coefficient of interactions between the stars in solution, is shifted with respect of the theta-point for linear polymers, $\upsilon = 0$, towards poorer solvent strength conditions, $\upsilon \leq 0$. In the framework of the blob model, the onset of the collapse of a star polymer as a whole corresponds to the collapse of the outermost coronal blobs. A further decrease in the solvent strength results in the formation of a region of virtually constant

concentration at the periphery of the star, see Fig. 1c. This concentration is determined by the local balance of binary attractive and ternary repulsive interactions. In a more dense central region, the stretching of the arms is controlled by ternary monomer–monomer interactions. Upon progressive decrease in solvent strength, the boundary between the collapsed and the theta-region shifts progressively towards the center of the star. The star acquires a conformation of a spherical globule with a uniform density of its monomers.

These theoretical predictions are in good agreement with experiments [142] on the collapse transition in dilute solutions of organosoluble star polymers, i.e., poly(styrene) stars in cyclohexane. In these experiments, the temperature was varied around the theta-point (ca. 34.5°C). Lowering the temperature corresponds to an inferior solvent strength of cyclohexane.

In water, the solubility of most of synthetic PEs (e.g. PMAA or polysulfonic acid) depends strongly on the presence of ionized groups. In other words, the monomers of most synthetic PEs are often intrinsically hydrophobic [143].

In contrast to organosoluble polymers, for most known water-based nonionic polymers, the quality of water as a solvent decreases upon an increase in temperature. This is known as LCST (lower critical solution temperature) behavior [144]. Experimental observations of LCST behavior (thermoinduced collapse) of neutral stars or spherical polymer brushes in water are rare [145, 146], and do not yet provide systematic relationships between the LCST and the degree of branching.

Furthermore, polymers such as PDMAEMA combine a weak polybase character with thermoresponsive properties: at high pH and low temperatures PDMAEMA is not ionized, but, nevertheless, is soluble in water. An increase in temperature, however, leads to an increase in the hydrophobicity of the monomers and, at $T \geq$ LCST, the unionized polymers collapse, lose solubility, and precipitate from aqueous solution [47].

In poor solvents, the conformations of charged macromolecules are controlled by the competition between short-ranged attractive monomer–monomer interactions and long-ranged electrostatic repulsions between ionized monomers. The first theory of the collapse transition in a single linear (quenched) PE chain was proposed by Khokhlov [147], who predicted a gradual collapse of a PE chain upon a decrease in the solvent strength. According to this theory, a partially collapsed PE chain acquires the conformation of a longitudinally uniform cylindrical ("cigar-like") globule. The collapse transition in a weak (pH-sensitive) PE chain was considered by Raphael and Joanny [148], who predicted an abrupt transition from a stretched to a collapsed globular state, because of the coupling between the conformations and the ionization of a weak PE chain. That is, a lower degree of ionization of the monomers is expected in the collapsed globular conformation.

The theory of Khokhlov [147] was revised by Dobrynin, Rubinstein and Obukhov [149], who demonstrated that a partially collapsed quenched PE chain acquires a "pearl-necklace" conformation, consisting of collapsed globular beads connected by stretched bridges. The pearl-necklace structure appears due to interplay of short-range monomer-monomer attraction with long range repulsion and is a manifestation of the Rayleigh instability constrained by the chain connectivity [158, 159].

The size of each globular bead is controlled by a balance between the excess interfacial free energy of a bead and the intrabead Coulombic repulsion. The length of the bridges (strings of thermal blobs) adjusts the Coulomb force of the interbead repulsion to a critical force at which the mechanical unfolding of a polymer globule occurs [152]. MC and MD simulations unambiguously indicated the formation of such a intramolecular pearl-necklaces structure in strongly dissociating PE chains, where the local collapse is due to short-range monomer–monomer attraction [153, 154].

The nonlinear branched topology is expected to introduce novel specific features in the collapse transition of individual charged macromolecules, due to the interplay between intra- and interbranch Coulomb repulsion. Conformations of intrinsically hydrophobic star-branched PE have been studied experimentally in the past decade [50, 51]. Recently synthesized PDMAEMA stars responsive to both pH and temperature [47, 48] are expected to undergo an intramolecular collapse transition as a response to the increase in temperature. The latter provokes a decrease in the solubility of the monomers in the star arms.

The theory of the collapse transition in star-like PEs was developed by Borisov et al. [155] and Ross and Pincus [156] on the basis of a box-like model, which assumes a fairly uniform concentration of the monomers within the star (see Sect. 5). This analysis suggested that, in contrast to a neutral polymer star, which collapses gradually upon a decrease in the solvent strength [141], the collapse of a PE star has a first-order nature and involves coexistence of the collapsed and swollen states.

In a salt-free solution, the onset of collapse transition in a PE star corresponds to the collapse of individual electrostatic blobs in the uniformly stretched arms of the star. An increase in the number of star branches, p, enhances interbranch Coulomb repulsions, and, thereby, decreases the electrostatic blob size. Therefore, the collapse transition is shifted towards poorer solvent conditions upon an increase in p.

The picture of the collapse transition in quenched PE star has been revised by Misra et al. [157], who proposed that microphase coexistence, between a collapsed core domain and a swollen corona may occur inside an individual PE star. An essential Ansatz of all the mean field theories developed in [155–157] is the preassumption that the PE star retains its spherically symmetrical configuration in a partially collapsed state. The collapse transition is described in terms of the evolution of radial density distribution as a function of the solvent quality.

In contrast to this, the scaling theory of the PE star collapse developed in [27] suggested that, instead of the formation of a collapsed core, a decrease in the solvent strength may provoke the formation of bundles by the sticking of individual branches to each other. The bundle formation reduces the excess interfacial free energy of the collapsed domains, without a significant penalty in terms of the intramolecular Coulomb repulsion. More recently, the formation of bundles was theoretically predicted in colloidal PE brushes [42].

An intriguing question is, however, whether the pearl necklace, or some other types of multidomain intramolecular structures of low symmetry, may correspond to the equilibrium conformation of a partially collapsed star-branched PE. This problem has been recently addressed by Kosovan et al. [158] by means of MD simulations.

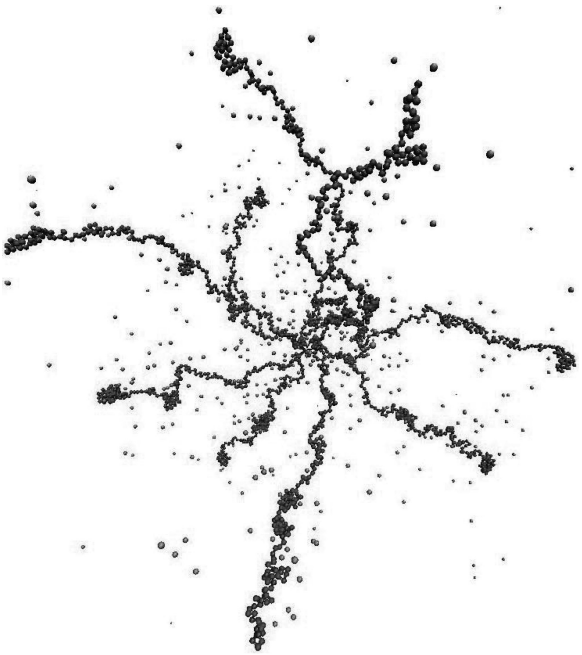

Fig. 19 MD simulation snapshot of a PE star in poor solvent; $p = 10$, $N = 200$, $\alpha = 0.25$

The simulations proved that a progressive decrease in the solvent quality induces a series of conformational transitions, giving rise to intramolecular multidomain structures of different morphologies. The pearl-necklace structures in separate branches are found at moderately poor solvent conditions. This structural motive persists for stars with a relatively small number of arms, also in the intermediate range of solvent quality. With inferior solvent strengths, the simulations provide evidence of sticking of individual branches/necklaces into bundles. The bundling is more pronounced in the central region of many-armed stars, whereas at the periphery of the star the bundles split into single-chain necklaces, Fig. 19. At sufficiently poor solvent strength, multiple intramolecular structures of different morphologies are observed in the simulations, i.e., the system is strongly frustrated. It is anticipated that this behavior is an inherent property of branched PEs, where the repulsive electrostatic interactions that operate on a large length scale compete with short-ranged attractions under the constraints of monomer connectivity in branched topologies.

9 Conclusions

We have presented an overview of theories that describe the conformations and solution properties of star-branched PEs. Whereas the principal qualitative results can be obtained on the basis of a simplified box-like cell model, systematic

treatments of the corresponding PB problem were achieved by employing the SF-SCF approach. The latter gives access to the partition function of stars in the self-consistent electrical field created by the charged arms in the presence of mobile counterions. Additional insights into counterion distributions in PE stars in both radial and angular directions are provided by MC and MD simulations.

The theoretical analysis proves that the majority of the counterions are localized inside the star, provided that the number of arms is large. The arm length has no significant influence on the degree of counterion localization. The PB analysis shows that the dimensionless electrostatic potential at the edge of the star corona drops almost to unity. Consequently, the counterions outside the corona are distributed fairly uniformly. The effective (renormalized) charge of the star, which determines the counterion concentration at the boundary of the Wigner–Seitz cell, approximately coincides with the total uncompensated charge Q^* within the star corona. The phenomenon of counterion localization in the intramolecular volume is typical for dilute salt-free solutions of highly branched polyions of arbitrary topology, including randomly branched, dendritic polyions, PE molecular brushes, etc.

The LEA can be applied to the analysis of conformations of PE stars with a sufficiently large number of arms. In contrast to neutral stars, for which the generalized Daoud–Cotton approach provides an accurate description of the star structure in terms of radial power law decay of polymer concentration and of local stretching of the arms, the nonlocal effects (related to the additional pulling force exerted by the terminal segments of the arms) are essential for PE stars in salt-free solutions.

Some peculiar effects arise in pH-sensitive stars because of a coupling between the conformations and the degree of ionization of the arms. In particular, the overall extension of the arms of the star depends in a non-monotonic fashion on the ionic strength in the bulk and on the number of the arms of the star.

The mean-spherical approximation provides an adequate description of the PE star conformation under conditions of good or theta-solvent. However, in contrast to some early theoretical predictions, simulations give evidence that conformational transition related to the collapse of hydrophobic or thermosensitive PE stars is accompanied by the formation of various intramolecular structures of low symmetry (pearl necklaces, bundles).

Experiments on PE stars show extremely low values of the osmotic coefficient in salt-free star solution, thus proving the concept of counterion localization. Potentiometric titration experiments confirm theoretical predictions concerning a shift of the effective pK_a upon an increase in the number of arms.

Acknowledgment The support of the European Union within the Marie Curie Research and Training Network POLYAMPHI and of the Russian Foundation for Basic Research, grant 08-03-33126a is gratefully acknowledged. OVB acknowledges the Alexander von Humboldt Foundation for support of his stay in the University of Bayreuth. We thank A.A. Polotsky, F.A. Plamper and P. Kosovan for creating Figs. 2,8, and 19, respectively.

Appendix: Local Electroneutrality Approximation

The local electroneutrality approximation (LEA) assumes that the local number density of charged monomer units in the PE corona is approximately equal to local (excess) number density of mobile counterions:

$$\sum_{j^-} c_{j^-}(r) + \alpha(r) c_{\mathrm{p}}(r) = \sum_{j^+} c_{j^+}(r) \tag{55}$$

We will focus on the case of a solution that contains, in addition to H^+ and OH^- ions (whose concentration is controlled by the pH in the bulk), also monovalent co- and counterions due to added salt (e.g., Na^+, Cl^-, etc.). Here, $c_j(r)$ is the local concentration of ions of type j, and $c_{\mathrm{p}}(r)$ and $\alpha(r)$ are the concentration of the monomer units and the degree of ionization in the corona at a distance r from the center of the star, respectively. Note that we assume that the star is negatively charged. The summation on the right-hand side of (55) includes all the cationic species (i.e. salt ions, c_{Na^+}, and hydrogen ions, c_{H^+}), whereas the summation on the left-hand side of (55) includes all the anionic species (i.e. salt ions, c_{Cl^-}, and hydroxyl ions, c_{OH^-}).

The concentrations c_{bj} (or, equivalently, the chemical potentials) of all the mobile ions are assumed to be constant in bulk solution, wherein the osmotic pressure is given by:

$$\Pi_{\mathrm{b}}/k_{\mathrm{B}}T = \Phi_{\mathrm{ion}} \equiv \sum_{j} c_{bj} \tag{56}$$

(Here, the summation is performed over all ion species including H^+ and OH^- ions).

In the framework of LEA, the electrostatic interactions manifest themselves through the entropy of ions disproportionated between the interior of a strongly branched macromolecule and bulk solution. Therefore, the driving force for swelling of a branched polyion can be formulated in terms of the differential osmotic pressure of small ions inside and outside of the macromolecule.

If the (excess) electrostatic potential $\Delta\Psi(r)$ is ascribed to the intramolecular volume of the star, then the concentrations of all mobile ions obey the Donnan rule (the Boltzmann law):

$$c_{j^-}(r)/c_{bj^-}(r) = c_{bj^+}(r)/c_{j^+}(r) = \exp(e\Delta\Psi(r)/k_{\mathrm{B}}T) \tag{57}$$

Note, that here all the small ions (co- and counterions) are assumed to be monovalent.

Combining (55) and (57), we find for the excess electrostatic potential:

$$\exp(e\Delta\Psi(r)/k_{\mathrm{B}}T) = \sqrt{1 + (\alpha(r)c_{\mathrm{p}}(r)/\Phi_{\mathrm{ion}})^2} - \alpha(r)c_{\mathrm{p}}(r)/\Phi_{\mathrm{ion}} \tag{58}$$

It follows from (57) and (58), that the total concentration of counterions inside the star is $\sum_{j^+} c_{j^+}(r) \cong \alpha(r)c_{\mathrm{p}}(r)$, provided that $\alpha(r)c_{\mathrm{p}}(r)/\sum_j c_{bj} \to \infty$. That is, in the

limit of low salt concentrations, the charge density created by the charged monomers is locally matched by that of the mobile counterions (osmotic regime).

Quenched Polyelectrolyte Corona

For a strongly dissociating (quenched) PE star, the density of the Gibbs free energy is given by:

$$f_{\text{ion,quenched}}\{c_{\text{p}}(r)\}/k_{\text{B}}T = \sum_j c_j(r)[\ln c_j(r) - 1] + \Pi_b/k_{\text{B}}T - \sum_j c_{bj}\ln c_{jb} =$$

$$\alpha_b c_{\text{p}}(r)\left(\left(1 - \sqrt{1 + (\alpha_{\text{b}} c_{\text{p}}(r)/\Phi_{\text{ion}})^2}\right)/(\alpha_b c_{\text{p}}(r)/\Phi_{\text{ion}})\right.$$

$$\left. + \text{Arsh}(\alpha_{\text{b}} c_{\text{p}}(r)/\Phi_{\text{ion}})\right) \tag{59}$$

where $\text{Arsh}(x) \equiv \ln(x + \sqrt{1+x^2})$. An expansion of $f_{\text{ion}}\{c_{\text{p}}(r)\}$ in series of $\alpha_b c_{\text{p}}(r)/\Phi_{\text{ion}}$ leads to the asymptotic power law dependencies:

$$\frac{f_{\text{ion}}\{c_{\text{p}}(r)\}}{k_{\text{B}}T} \cong \begin{cases} \alpha_{\text{b}} c_{\text{p}}(r)\ln(2\alpha_b c_{\text{p}}(r)/e\Phi_{\text{ion}}), & \alpha_b c_{\text{p}}(r)/\Phi_{\text{ion}} \gg 1 \\ \frac{\alpha_{\text{b}}^2 c_{\text{p}}^2(r)}{2\Phi_{\text{ion}}}, & \alpha_{\text{b}} c_{\text{p}}(r)/\Phi_{\text{ion}} \ll 1 \end{cases} \tag{60}$$

corresponding to the limits of low and high salt concentrations, respectively. As follows from (60), at low concentrations of added salt the free energy is dominated by the translational entropy of the counterions that are confined inside the PE corona. When the concentration of added ions far exceeds the average concentration of counterions in the PE corona (salt-dominated regime), the differential swelling pressure of the counterions can be described as excluded-volume (binary) monomer–monomer interactions with an effective second viral coefficient $\upsilon_{\text{eff}} = \alpha^2/2\Phi_{\text{ion}}$.

Annealing Polyelectrolyte Corona

For an annealing (weakly dissociating) PE star, one has to account for the shift in the local ionization equilibrium, whose free energy cost, $f_{\text{ionization}}$, must complement the free energy of the star:

$$f_{\text{ionization}}\{c_{\text{p}}(r)\}/k_{\text{B}}T = c_{\text{p}}(r)$$

$$\left[\alpha(r)\ln\alpha(r) + (1-\alpha(r))\ln(1-\alpha(r)) - \alpha(r)\ln\frac{K_a}{c_{\text{bH}^+}}\right] \tag{61}$$

This leads to:

$$f_{\text{ion,annealing}}\{c_{\text{p}}(r)\}/k_{\text{B}}T = \left(1-\sqrt{1+(\alpha(r)c_{\text{p}}(r)/\Phi_{\text{ion}})^2}\right)\Phi_{\text{ion}} + c_{\text{p}}(r)\ln\left(1-\alpha(r)\right) \tag{62}$$

where $\alpha(r) = \alpha\{c_{\text{p}}(r), \Phi_{\text{ion}}\}$ is determined by the following equation:

$$\frac{\alpha(r)}{1-\alpha(r)}\cdot\frac{1-\alpha_{\text{b}}}{\alpha_{\text{b}}} = \sqrt{1+(\alpha(r)c_{\text{p}}(r)/\Phi_{\text{ion}})^2} - \alpha(r)c_{\text{p}}(r)/\Phi_{\text{ion}} \tag{63}$$

and α_{b} is the degree of ionization of an isolated acidic monomer in the bulk solution at given pH. The detailed derivation of the free energy density for the annealing PE corona can be found in [159].

Equations (62) and (63) can be expanded in series of $\alpha(r)c_{\text{p}}(r)/\Phi_{\text{ion}}$, and the logarithm in (62) can be expanded up to linear order in $\alpha(r) \ll 1$. As a result, one gets:

$$\alpha(r) \cong \begin{cases} \left(\frac{\alpha_{\text{b}}}{1-\alpha_{\text{b}}}\cdot\frac{\Phi_{\text{ion}}}{2c_{\text{p}}(r)}\right)^{1/2}, & \alpha(r)c_{\text{p}}(r)/\Phi_{\text{ion}} \gg 1 \\ \alpha_{\text{b}}, & \alpha(r)c_{\text{p}}(r)/\Phi_{\text{ion}} \ll 1 \end{cases} \tag{64}$$

and:

$$\frac{f_{\text{ion}}\{c_{\text{p}}(r)\}}{k_{\text{B}}T} \cong \begin{cases} -\left(\frac{2\alpha_{\text{b}}}{1-\alpha_{\text{b}}}\Phi_{\text{ion}}c_{\text{p}}(r)\right)^{1/2}, & \alpha(r)c_{\text{p}}(r)/\Phi_{\text{ion}} \gg 1 \\ \frac{\alpha_{\text{b}}^2 c_{\text{p}}^2(r)}{2\Phi_{\text{ion}}} + c_{\text{p}}(r)\ln\left(1-\alpha_b\right), & \alpha(r)c_{\text{p}}(r)/\Phi_{\text{ion}} \ll 1 \end{cases} \tag{65}$$

As follows from (64), at low salt concentrations (annealing osmotic regime), the degree of ionization of the monomers in the corona is an increasing function of the salt concentration, Φ_{ion} and a decreasing function of local polymer concentration, $c_{\text{p}}(r)$.

References

1. Oosawa F (1971) Polyelectrolytes. Dekker, New York
2. Barrat JL, Joanny JF (1996) In: Prigogine I, Rice SA (eds) Advances in chemical physics. Wiley, New York
3. Dobrynin AV, Rubinstein M (2005) Pogr Polym Sci 30:1049
4. Ballauff M, Borisov OV (2006) Curr Opin Colloid Interface Sci 11:316
5. Ballauff M, Likos C (2004) Angew Chem Intl Ed 43:2998
6. Peppas NA (1997) Curr Opin Colloid Interface Sci 2:531
7. Mori H, Müller AHE (2003) Prog Polym Sci 28:1403
8. Zhang M, Müller AHE (2005) J Polym Sci Part A Polym Chem 43:3461
9. Xu Y, Plamper F, Ballauff M, Müller AHE (2010) Adv Polym Sci 228:1
10. Förster S, Abetz V, Müller AHE (2004) Adv Polym Sci 166:173
11. Abu-Lail NI, Camesano TA (2003) Biomacromolecules 4:1000

12. Ng L, Grodzinsky AJ, Patwari P, Sandy J, Plaas A, Ortiz C (2003) J Struct Biol 143:242
13. Fuchs E, Cleveland DW (1998) Science 279:514
14. Burchard W (1999) Adv Polym Sci 143:113
15. Birshtein TM, Mercurieva AA, Leermakers FAM, Rud OV (2008) Polym Sci A(Russia) 50:1673
16. Stockmayer WH, Zimm BH (1949) J Chem Phys 17:301
17. Benoit H (1953) J Polym Sci 11:507
18. Benoit H (1955) R Acad Sci 533
19. Candau F, Rempp R, Benoit H (1972) Macromolecules 5:627
20. Khokhlov AR (1978) Polymer 19:1387
21. Daoud M, Cotton JP (1982) J Phys (France) 43:531
22. Zhulina EB (1984) Polym Sci USSR 26:794
23. Birshtein TM, Zhulina EB (1984) Polymer 25:1453
24. Birshtein TM, Zhulina EB, Borisov OV (1986) Polymer 27:1079
25. Manning G (1969) J Chem Phys 51:3249
26. Pincus P (1991) Macromolecules 24:2912
27. Borisov OV (1996) J Phys II (France) 6:1
28. Borisov OV, Zhulina EB (1998) Europ Phys J B 4:205
29. Klein Wolterink J, Leermakers FAM, Fleer GJ, Koopal LK, Zhulina EB, Borisov OV (1999) Macromolecules 32:2365
30. Klein Wolterink J, van Male J, Cohen Stuart MA, Koopal LK, Zhulina EB, Borisov OV (2002) Macromolecules 35:9176
31. Borisov OV, Vilgis TA (1996) Europhys Lett 35:327
32. Borisov OV, Daoud M (2001) Macromolecules 34:8286
33. Klein Wolterink J, van Male J, Daoud M, Borisov OV (2003) Macromolecules 36:6624
34. Kramarenko EYu, Khokhlov AR, Yoshikawa K (1997) Macromolecules 30:3383
35. Levin Y, Deihl A, Fernandez-Nieves A, Fernandez-Barbero A (2002) Phys Rev E 65:036143
36. Alexander S, Chaikin PM, Grant P, Morales GJ, Pincus P, Hone D (1984) J Chem Phys 80:5776
37. Leermakers FAM, Ballauff M, Borisov OV (2008) Langmuir 24:10026
38. Roger M, Guenoun P, Muller F, et al (2002) Eur Phys J E 9:313
39. Jusufi A, Likos CN, Löwen H (2002) J Chem Phys 116:11011
40. Jusufi A, Likos CN, Ballauff M (2004) J Colloid Polym Sci 282: 910
41. Mei Y, Hoffmann M, Ballauff M, Jusufi A (2008) Phys Rev E 77:031805
42. Sandberg DJ, Carillo JY, Dobrynin AV (2007) Langmuir 23:12716
43. Plamper FA, Becker H, Lanzendörfer M, Patel M, Wittemann A, Ballauff M, Müller AHE (2005) Macromol Chem Phys 206:1813
44. Ballauff M (2007) Prog Polym Sci 32:1135
45. Guo X, Ballauff M (2001) Phys Rev E 64:015406
46. Karaky K, Reynaud S, Billon L, Francois J, Chreim Y (2005) J Polym Sci Part A Polym Chem 43:5186
47. Plamper FA, Ruppel M, Schmalz A, Borisov OV, Ballauff M, Müller AHE (2007) Macromolecules 40:8361
48. Plamper FA, Schmalz A, Penott-Chang E, Drechsler M, Jusufi A, Ballauff M, Müller AHE (2007) Macromolecules 40:5689
49. Plamper FA, Walther A, Müller AHE, Ballauff M (2007) Nano Lett 7:167
50. Mays JW (1990) Polym Commun 31:170
51. Heinrich M, Rawiso M, Zilliox JG, Lesieur P, Simon JP (2001) Eur Phys J E 4:131
52. Muller F, Guenoun P, Delsanti M, Deme B, Auvray L, Yang J, Mays JW (2004) Eur Phys J E 15:465
53. Muller F, Delsanti M, Auvray L, Yang J, Chen YJ, Mays JW, Demé B, Tirrell M, Guenoun P (2000) Eur Phys J E 3:45
54. Amiel C, Sikka M, Schneider JW, Tsao YH, Tirrell M, Mays JW (1995) Macromolecules 28:3125

55. Guenoun P, Delsanti M, Gaseau D, Auvray L, Cook DC, Mays JW, Tirrell M (1998) Eur Phys J B 1:77
56. Guenoun P, Davis HT, Tirrell M, Mays JW (1996) Macromolecules 29:3965
57. Guenoun P, Muller F, Delsanti M, Auvray L, Chen YJ, Mays JW, Tirrell M (1998) Phys Rev Lett 81:3872
58. Van der Maarel JRC, Groenewegen W, Egelhaaf SU, Lapp A (2000) Langmuir 16:7510
59. Groenewegen W, Egelhaalf SU, Lapp A, van der Maarel JRC (2000) Macromolecules 33:3283
60. Groenewegen W, Lapp A, Egelhaalf SU, van der Maarel JRC (2000) Macromolecules 33:4080
61. Kiserow D, Prochazka K, Ramireddy C, Tuzar Z, Munk P, Webber SE (1992) Macromolecules 25:461
62. Khougaz K, Astafieva I, Eisenberg A (1995) Macromolecules 28:7135
63. Förster S, Hemsdorf N, Leube W, Schnablegger H, Regenbrecht M, Akari S, Lindner P, Böttcher C (1999) J Phys Chem 103:6657
64. de Gennes PG (1979) Scaling concepts in polymer physics. Cornell University Press, Ithaca
65. Alexander S (1977) J Phys (France) 38:983
66. de Gennes PG (1980) Macromolecules 13:1069
67. Pincus P (1976) Macromolecules 9:386
68. Grest GA, Kremer K, Milner ST, Witten TA (1989) Macromolecules 22:1904
69. Grest GA (1994) Macromolecules 27:3493
70. Zifferer G (1999) Macromol Theory Simul 8:433
71. Havrankova J, Limpouchova Z, Prochaska K (2003) Macromol Theory Simul 12:512
72. Hsu HP, Nadler W, Grassberger P (2004) Macromolecules 37:4658
73. Förster S, Burger C (1998) Macromolecules 31:879
74. Bauer BI, Hadjichristidis N, Fetters LI, Roovers JE (1980) J Am Chem Soc 102:2410
75. Willner L, Jacknischke O, Richter D, Roovers J, Zhou LL, Toporowski PM, Fetters LJ, Huang JS, Lin MY, Hadjichrisitidis N (1994) Macromoleules 27:3821
76. Stellbrink J, Willner L, Richter D, Lindner P, Fetters LJ, Huang JS (1999) Macromoleules 32:5321
77. Cogan CA, Gast AP, Capel M (1991) Macromolecules 24:6512
78. Cogan CA, Gast AP, Butun V, Armes SP (1999) Macromolecules 32:4302
79. Held D, Müller AHE (2000) Macromol Symp 157:225
80. Witten TA, Pincus P (1986) Macromolecules 19:2509
81. Witten TA, Pincus PA, Cates ME (1986) Europhys Lett 2:137
82. Likos CN, Löwen H, Watzlawek M, Abbas B, Jucknischke O, Allgaier J, Richter D (1998) Phys Rev Lett 80:4450
83. Likos CN (2001) Phys Rep 348:267
84. Jusufi A, Likos CN (2009) Rev Mod Phys 81:1753
85. Marques CM, Izzo D, Charitat T, Mendes E (1998) Europ Phys J B 3:353
86. Beaudoin E, Borisov OV, Lapp A, Billon L, Hiorns RC, Francois J (2002) Macromolecules 35:7436
87. Beaudoin E, Borisov OV, Lapp A, Francois J (2003) Macromol Symp 191:89
88. Odijk T (1977) J Polym Sci Polym Phys Ed 15:447
89. Skolnick J, Fixman M (1977) Macromolecules 12:688
90. Flory PJ (1953) Principles of polymer chemistry. Cornell University Press, Ithaca
91. de Gennes PG, Pincus P, Velasco RM, Brochard F (1976) J Phys (France) 37:1461
92. Khokhlov AR, Khachaturian KA (1982) Polymer 23:1742
93. Shusharina NA, Rubinstein M (2008) Macromolecules 41:203
94. Kegler K, Salomo M, Kremer F (2007) Phys Rev Lett 98:058304
95. Kegler K, Konieczny M, Dominguez-Espinosa G, Gutsche C, Salomo M, Kremer F, Likos CN (2008) Phys Rev Lett 100:118302
96. Dominguez-Espinosa G, Synytska A, Drechsler A, Gutsche C, Kegler K, Uhlmann P, Stamm M, Kremer F (2008) Polymer 49:4802

97. Elmahdy MM, Synytska A, Drechsler A, Gutsche C, Uhlmann P, Stamm M, Kremer F (2009) Macromolecules 42:9096
98. Zhulina EB, Borisov OV (1997) J Chem Phys 107:5952
99. Isaacson J, Lubensky TC (1980) J Phys Lett 41:L-469
100. Daoud M, Joanny JF (1981) J Phys (France) 42:1359
101. Zimm BH, Stockmayer WH (1949) J Chem Phys 17:1301
102. Birshtein TM, Borisov OV, Zhulina EB, Khokhlov AR, Yurasova TA (1987) Polym Sci USSR 29:1293
103. Fredrickson G (1993) Macromolecules 26:2825
104. Rouault Y, Borisov OV (1996) Macromolecules 29:2605
105. Feuz L, Leermakers FAM, Textor M, Borisov OV (2005) Macromolecules 38:8891
106. Feuz L, Strunz P, Geue T, Textor M, Borisov OV (2007) Europ Phys J E 23:237
107. Hsu H-P, Paul W, Binder K (2010) Macromolecules 43:3094
108. Kiani C, Chen L, Wu YJ, Yee AJ, Yang BB (2002) Cell Res 12:19
109. Thornton DJ, Rousseau K, McGuckin MA (2008) Annu Rev Physiol 70:459
110. Janmey PA, Leterrier J-F, Herrmann H (2003) Curr Opin Colloid Interface Sci 8:40
111. Jones JB, Safinya CR (2008) Biophys J 95:723
112. Beck R, Deek J, Jones JB, Safinya CR (2010) Nat Mater 9:40
113. Mukhopadhyay R, Kumar S, Hoh JH (2004) BioEssays 26:1
114. Zhulina EB, Leermakers FAM (2009) Soft Matter 5:2836
115. Zhulina EB, Leermakers FAM (2007) Biophys J 93:1421
116. Zhulina EB, Leermakers FAM (2007) Biophys J 93:1452
117. Zhulina EB, Leermakers FAM (2010) Biophys 98:462
118. Leermakers FAM, Zhulina EB (2008) BRL 3:459
119. Leermakers FAM, Zhulina EB (2010) Eur Biophys J 39:1323
120. Fleer GJ, Cohen Stuart MA, Scheutjens JMHM, Cosgrove T, Vincent B (1993) Polymers at interfaces. Chapman and Hall, London
121. Borisov OV, Zhulina EB (1997) J Phys II 7:449
122. Semenov AN (1985) Sov Phys JETP 61:733
123. Zhulina EB, Birshtein TM, Borisov OV (2006) Eur Phys J E 20:243
124. Wijmans CM, Zhulina EB (1993) Macromolecules 26:7214
125. Dobrynin AV, Colby RH, Rubinstein M (1995) Macromolecules 28:1859
126. Zhulina EB, Birshtein TM, Borisov OV (1995) Macromolecules 28:1491
127. Wesley RD, Cosgrove T, Thompson L, Armes SP, Billingham NC, Baines FL (2000) Langmuir 16:4467
128. Prinz C, Muller P, Maaloum M (2000) Macromolecules 33:4896
129. Currie EPK, Sieval AB, Fleer GJ; Cohen Stuart MA (2000) Langmuir 16:8324
130. Biesalski M, Johannsmann D, Ruhe J (2002) J Chem Phys 117:4988
131. Matejicek P, Podhajewcka K, Humpolickova J, Uhlik F, Jelinek K, Limpouchova Z, Prochazka K (2004) Macromolecules 37:10141
132. Konradi R, Ruhe J (2005) Macromolecules 38:4345
133. Zhang HN, Ruhe J (2005) Macromolecules 38:4855
134. Xu L, Zhu Z, Borisov OV, Zhulina EB, Sukhishvili SA (2009) Phys Rev Lett 103:N118301
135. Zhulina EB, Borisov OV, Birshtein TM (1999) Macromolecules 32:8189
136. Birshtein TM, Zhulina EB (1996) Ber Bunsen Phys Chem 100:929
137. Mei Y, Lauterbach K, Hoffmann M, Borisov OV, Ballauff M, Jusufi A (2006) Phys Rev Let 97:158301
138. Toomey R, Tirrell M (2008) Annu Rev Phys Chem 59:493
139. Castelnovo M, Evilevitch A (2006) Europhys Lett 73:635
140. Borisov OV, Birshtein TM, Zhulina EB (1988) Polym Sci USSR 30:772
141. Zhulina EB, Borisov OV, Birshtein TM (1988) Polym Sci USSR 30:780
142. Meunier JC, Leemput R (1971) Makromolek Chem B147:191
143. Williams CE, Wafa E (1995) J Phys II (France) 5:1269
144. Aseyev VO, Tenhu H, Winnik FM (2006) Adv Poly Sci 196:1
145. Zeng Q, Pan CY (2006) Eur Polym J 42: 807

146. Lu Y, Witteman A, Ballauff M, Drechsler M (2006) Macromol Rapid Commun 27:1137
147. Khokhlov AR (1980) J Phys A 13:979
148. Raphael E, Joanny JF (1990) Europhys Lett 13:623
149. Dobrynin AV, Rubinstein M, Obukhov SP (1996) Macromolecules 29:2974
150. Lord Rayleigh (1882) Phil Mag 14:184
151. Borisov OV, Zhulina EB (2005) Macromolecules 38:2506
152. Halperin A, Zhulina EB (1991) Europhys Lett 15:417
153. Lyulin AV, Dünweg B, Borisov OV, Darinskii AA (1999) Macromolecules 32:3264
154. Micka U, Holm C, Kremer K (1999) Langmuir 15:4033
155. Borisov OV, Birshtein TM, Zhulina EB (1992) Prog Colloid Polym Sci 90:177
156. Ross R, Pincus P (1992) Macromolecules 25:2177
157. Misra S, Mattice WL, Napper DH (1994) Macromolecules 27:7090
158. Kosovan P, Kuldova J, Limpouchova Z, Prochazka K, Zhulina EB, Borisov OV (2010) Soft Matter 6:1872
159. Zhulina EB, Borisov OV (2002) Macromolecules 35:9191